DANISH METEOROLOGICAL INSTITUTE

——— SCIENTIFIC REPORT ———

02-13

Precipitation hindcasts of historical flood events

Kai Sattler

COPENHAGEN 2002

ISSN Nr. 0905-3263 (printed)
ISSN Nr. 1399-1949 (online)
ISBN-Nr. 87-7478-467-6

Precipitation hindcasts of historical flood events

Kai Sattler

Danish Meteorological Institute

Scientific Report 02-13

Abstract

This report describes three deterministic hindcasts of historical heavy rain events, which were performed at the Danish Meteorological Institute (DMI) within the frame of the European project "An European Flood Forecasting system" (EFFS). The periods for the selected hindcasts were identified by the project consortium, and they cover different river basins as well as different seasons. Hindcasts of 72 hours lead time were performed for each day of these periods. A validation over the affected river basins reveals DMI-HIRLAM's abilities to forecast rain area and medium rain volumes. Large rain volumes tend to be under-predicted by the model. The heavy rain cases also show the difficulties arising from non-systematic prediction errors, where especially location errors of the rain area have decisive consequences on the prediction of precipitated water over a small river basin.

Contents

1 Introduction **3**

2 The NWP Model **4**

2.1 General setup and model domain 4

2.2 Hindcast configuration and post-processing 5

3 Historical Hindcasts **7**

3.1 The Piemonte flooding in 1994 7

3.2 The Rhine/Meuse flooding in 1995 9

3.3 The Odra flooding in 1997 11

4 Results **13**

4.1 The Piemonte case 1994 13

4.2 The Rhine/Meuse case 1995 15

4.3 The Odra case 1997 19

5 Conclusions and Outlook **25**

References **27**

1 Introduction

The EU-project ”An European Flood Forecasting System (EFFS)” aims at developing a prototype of a flood forecasting system for the European countries for up to 10 days in advance. The main emphasis is on the medium range lead time. Deterministic as well as probabilistic forecasts shall supply the meteorological input for the hydrological models. The European Centre for Medium-Range Weather Forecasts (ECMWF) shall supply medium range meteorological data from their deterministic model as well as from the Ensemble prediction system (EPS). Besides this, deterministic high resolution short range forecasts from the two European weather services Deutscher Wetterdienst (DWD) and Danish Meteorological Institute (DMI) are utilized, too. They make it possible to estimate the impact of horizontal resolution of the atmospheric predictions on water level forecasts. In addition, DMI is experimenting with mini ensembles in order to address uncertainties in the precipitation forecasts. The latter is not included in this report.

In order to test the methods and approaches of the flood forecasting system, historical flooding events are investigated. Three such events were identified by the project consortium. They comprise:

- The severe flooding in the Piemonte region in North Italy in November 1994, affecting the rivers Po and Reno
- The Rhine/Meuse flooding in December 1994 and January 1995
- The severe Odra flooding in Poland in July 1997

The periods of these floodings typically cover several weeks (see below), within which strong precipitation events occurred. ECMWF supplies meteorological data for these events from its meteorological archive. The DWD as well as DMI perform high resolution deterministic hindcasts in the short range with lead times up to 3 days ahead. From these hindcasts, a set of surface variables including large scale and convective precipitation amounts has been transferred for use in the hydrological models.

The following report describes the deterministic historical hindcasts performed at DMI. The first chapter describes the DMI-HIRLAM model used for the hindcasts as well as its configuration. In the second chapter, the historical rain events leading to the floods will be outlined. The third chapter shows results from the hindcasts including a comparison to precipitation analysis, and conclusions will be given in the last chapter.

2 The NWP Model

2.1 General setup and model domain

The HIgh Resolution Limited-Area Model (HIRLAM) is a numerical weather prediction (NWP) system for analysis and simulation of mesoscale dynamical and physical processes in the atmosphere. It has been developed within the international HIRLAM cooperation and describes the atmospheric equations of motion, energy and mass conservation in a discrete and approximated way (Källén, 1996). The DMI-HIRLAM has been used operationally at DMI for years. It is utilized to perform the historical hindcasts selected by the meteorological and hydrological partners of the EFFS project. HIRLAM is a hydrostatic grid-point model with a high spatial resolution, and it includes several parameterization models for the treatment of sub-grid physical processes. The atmospheric equations of motion, continuity of mass and conservation for energy and humidity are discretized on an ARAKAWA-C grid with hybrid vertical levels, and Eulerian as well as semi-Lagrangian treatment of advection is possible. Physical parameterizations include several turbulence schemes, different schemes for convection and condensation, a radiation scheme based on Savijärvi (1990) and surface flux parameterization using a drag formulation. Time integration is performed using a semi-implicit scheme, and a split time stepping of the physical parameterizations and the model dynamics is possible, which allows for larger time steps in the physics with respect to the model dynamics time step. The DMI-HIRLAM model system, as it was applied in this work, is described in detail by Sass et al. (2000).

The basic configuration of the model is similar to that used operationally at DMI, i. e. the same physical parameterizations are used for the hindcasts as are in operational use. They comprise the Soft Transition condensation and convection scheme (STRACO, Sass et al. (1997) and Sass et al. (2000)), the turbulent kinetic energy (TKE) turbulence scheme of Cuxart et al. (2000), the radiation scheme of Savijärvi (1990), and the simple surface scheme as described in Sass et al. (2000). The lower boundary model topography is derived from the physiographic data base of the HIRLAM model.

In order to suit the needs within the project, and under consideration of available computational resources, a doubly 1-way nested model setup has been established, which is based on the global model of ECMWF (Fig. 1).

The first DMI-HIRLAM model is established with 0.3° horizontal grid spacing and uses 31 vertical levels. It is initialized by ECMWF analysis data from 12 UTC. Its lateral boundaries are updated by the ECMWF forecasts with a 6 hour frequency, using time interpolation in order to assure smooth transition phases. The model utilizes semi-Lagrangian advection. This permits a time step of 450s in the dynamics, and for the physical parameterizations, 900s have been chosen. The communicated parameters from the ECMWF analysis include all prognostic variables on the model levels of the ECMWF model, except cloud water and TKE (Fig. 1).

The second DMI-HIRLAM model is established on a grid with 0.1° horizontal grid spacing and also with 31 vertical levels, the latter with a similar structure as before. It is initialized by the 0.3° DMI-HIRLAM model, and updated hourly at its lateral boundaries by this model. The 0.1° DMI-HIRLAM model utilizes the Eulerian advection scheme and runs with about 60s time step for the dynam-

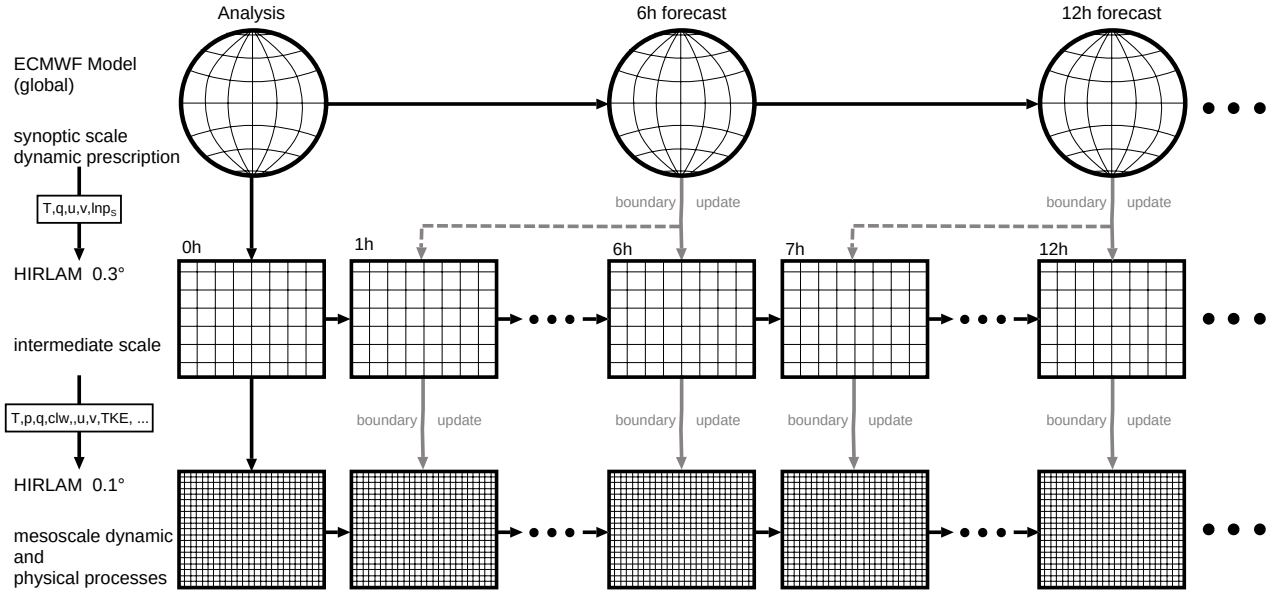

FIG. 1: Sketch of the DMI-HIRLAM model setup for the historical hindcasts. The large scale host model is the ECMWF global model, where 6 hourly boundary data are available to the intermediate model. The high-resolution model is updated every hour at its boundaries by the intermediate model.

ics. The time step for the physical parameterizations has been chosen to 540s. The communicated variables between the first and the second DMI-HIRLAM model include all prognostic model variables. The forecasts from the 0.1° DMI-HIRLAM model cover the European area and forecast results are transferred for utilization in the hydrological models. The variables, which are stored for this purpose comprise:

- accumulated precipitation (stratiform and convective)
- 2 metre temperature
- 2 metre dew point temperature
- 10 metre wind speed
- accumulated surface latent heat flux
- soil moisture of the top soil layer

The respective domains covered by the two DMI-HIRLAM models are shown in Fig. 2. The grid representation is in rotated latitude-longitude coordinates. In addition to the depicted domains relaxation zones at the lateral boundaries have been set to 15 grid points in width.

The lower boundaries of the two models are prescribed using data from the DMI-HIRLAM climate generation system (Sattler, 1999).

2.2 Hindcast configuration and post-processing

The hindcasts for the historical heavy rain events were performed on a daily basis. A run was started at 12 UTC each day within the respective period of the event (see Sec. 3). The hindcast length was 72 hours. The hindcast fields were written hourly, including the variables listed above. This

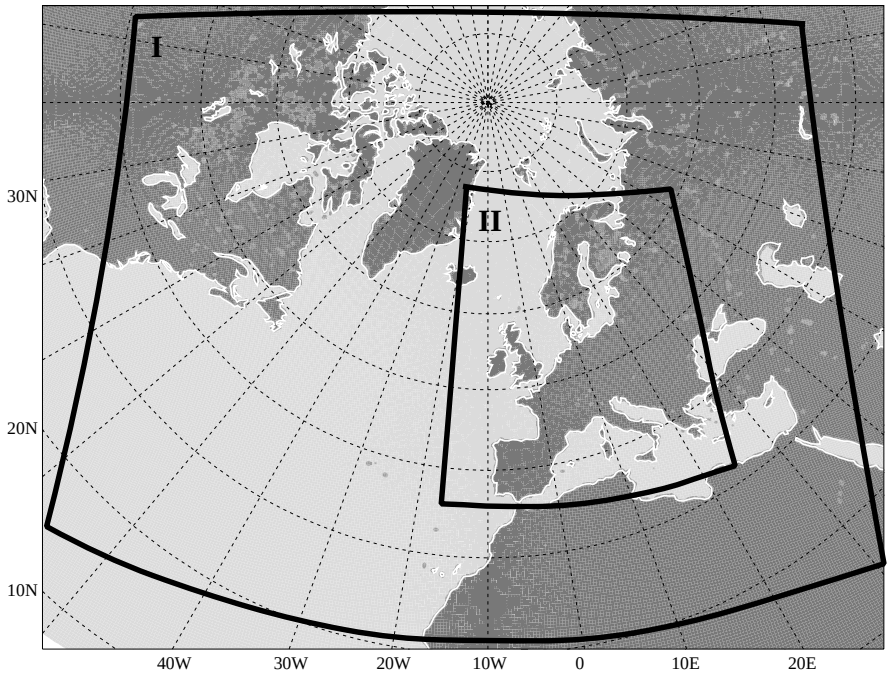

FIG. 2: Regions covered by the two DMI-HIRLAM models used in the historical hindcasts. The outer model domain (I) is covered by a 0.3°-grid, while the inner domain (II) is covered by a 0.1°-grid. The inner model covers all important river catchments of Europe.

configuration results in three ”forecasts” for a 24 hour period, referring to a prediction of 0–24 hours, 24–48 hours and to 48–72 hours, respectively.

In order to validate the hindcasts, data from a precipitation analysis performed at the DWD were utilized. The precipitation analysis is performed on the grid of the German ”Lokal-Modell” LM (Doms and Schättler, 1999) and is mainly based on observation data from synoptical as well as climatological stations, the latter of which make up a significantly denser network of precipitation observations than the synoptic stations. In the case of the Piemonte flooding of November 1994, DWD utilized additional rainfall data from the Mesoscale Alpine Project MAP (MAP, 2002) in their analyses.

Even though the analyses data for the three historical events do not cover the historical periods completely, the most important time ranges are included.

3 Historical Hindcasts

The three historical events regarded here led to severe river floodings in three different European regions (see Fig. 3). They where connected to or triggered by one or more events of heavy precipitation with several days of duration. The following outlines describe briefly some meteorological aspects of these precipitation events and identify the periods chosen for the DMI-HIRLAM hindcasts.

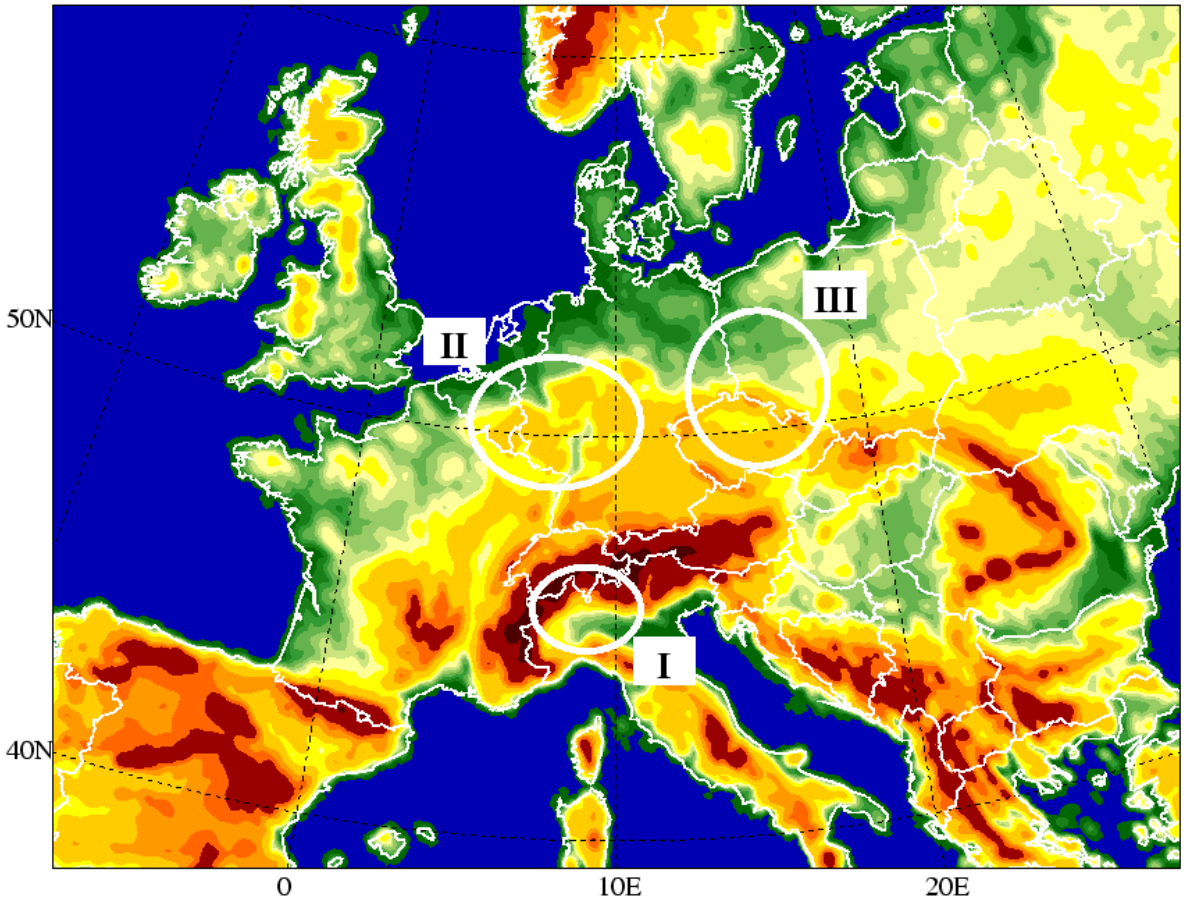

FIG. 3: Location of the three precipitation events leading to river flooding.

3.1 The Piemonte flooding in 1994

Large amounts of precipitation occurred in November 1994 in the Piemonte region in the North-Western part of Italy (I in Fig. 3). As can be seen from meteorological observations located in the affected area (Fig. 4), the large rainfall amounts were mainly due to one major precipitation event, which was observed between 5^{th} and 6^{th} of November 1994 (Fig. 5). This event was connected to a small depression developing over the Balearic Islands from a baroclinically unstable trough positioned over the Western Europe. The path of the depression crossed the Alps from south, resulting in an enhancement of precipitation south of the alpine chain to extreme values by orographic forcing. This caused a severe flood over the western part of the Po river basin, the Piemonte region (Buzzi et al., 1995).

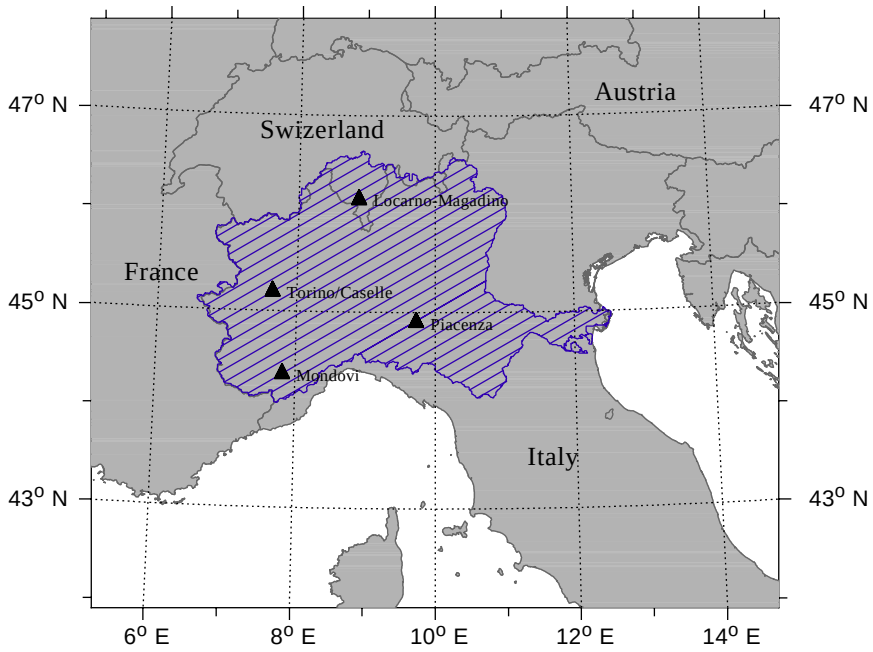

FIG. 4: Location of the four stations, which observed the largest rainfall amounts over the shown period. The river basin of the Po river is depicted by the hatched area.

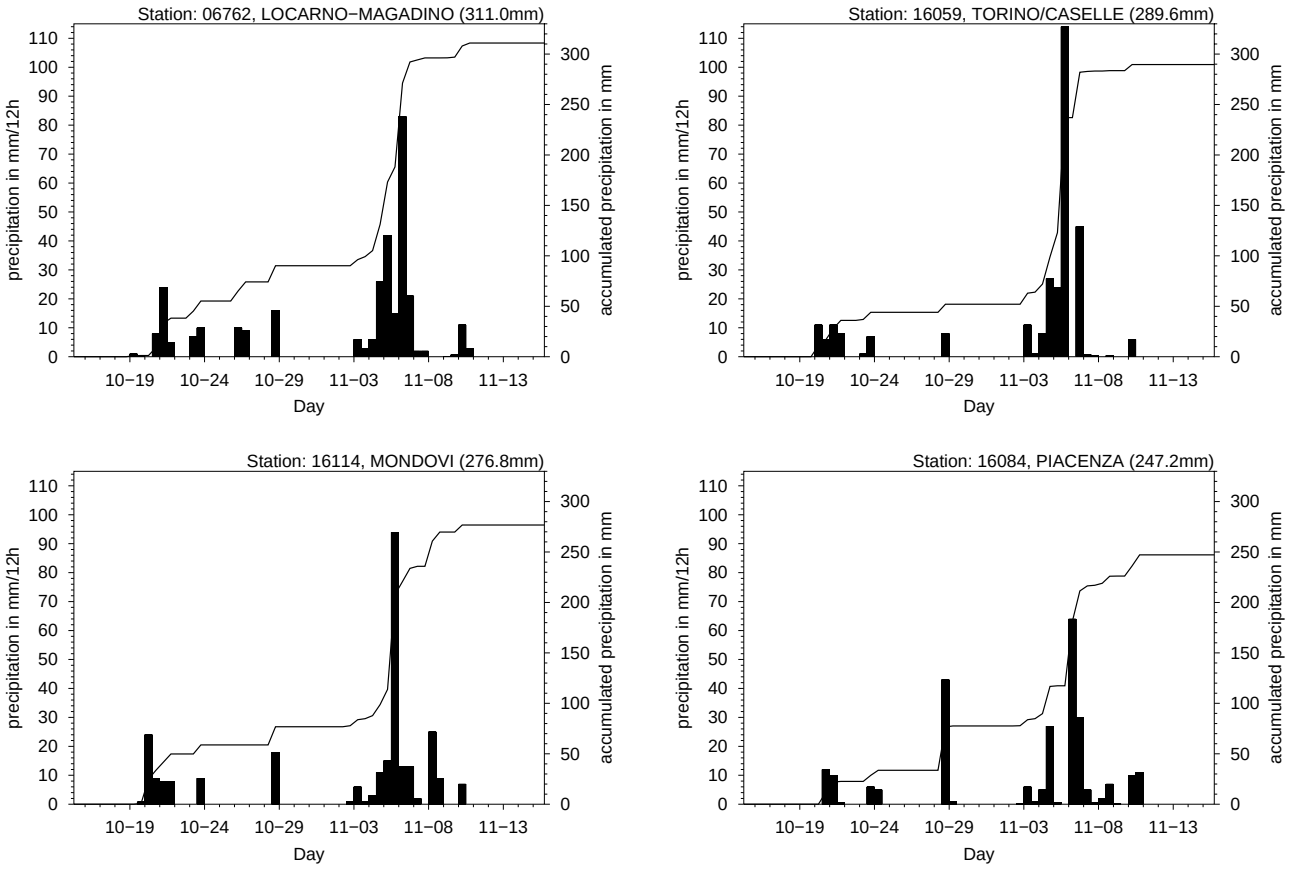

FIG. 5: Observed 12 hourly accumulated precipitation (columns, left ordinate) and pluviographs (curves, right ordinate) of the four synoptic meteorological stations Locarno-Magadino (upper left), Torino/Caselle (upper right), Mondovi (lower left) and Piacenza (lower right). The depicted period comprises the days between 15$^{\mathrm{th}}$ of October to 15$^{\mathrm{th}}$ of November 1994.

The meteorological stations indicated in Fig. 4 were beyond those registering the largest precipitation amounts. The stations are located in the western part of the Po river basin, the Piemonte region. The precipitation observations from these stations are shown in Fig. 5. The event was neither preceded or succeeded by another heavy rain event, and it resulted locally in more than 250 mm observed precipitation.

The period selected for the hindcasts of the Piemonte flooding comprises 15^{th} of October 1994 to 15^{th} of November 1994, each day of which covered by a hindcast with 3 days lead time. Precipitation analysis data for this event was available from the 1^{st} to the 12^{th} of November 1994. The DMI-HIRLAM is used in the hindcasts as described in Sec. 2.

3.2 The Rhine/Meuse flooding in 1995

This flood occurred in January 1995 and affected the rivers Rhine and Meuse (Meijgaard (1995) and Fink et al. (1995)), see also II in Fig. 3. Contrary to the case in the Piemonte area, the river floods were, besides hydrological causes, linked to a series of precipitation events with a larger spatio-temporal extent than in the first case.

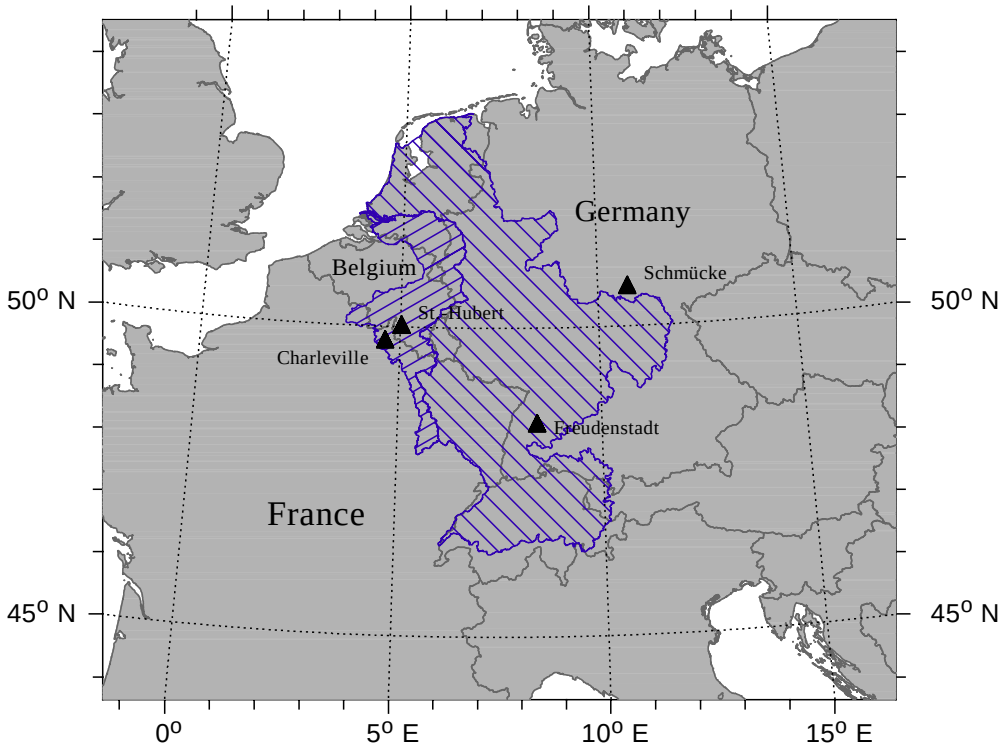

FIG. 6: Location of the four stations, which observed the largest rainfall amounts over the shown period. The river basin of the rivers Rhine and Meuse are depicted by the hatched areas.

The events occurred over several weeks, each event being of rather medium than of extreme strength. This becomes clear when looking at some of the meteorological observations over the areas of the two river basins. Fig. 6 shows a map with the locations of four of the most significant synoptic observations, which measured the largest rainfall amounts over a period of more than five weeks (Fig. 7). As can be seen from Fig. 6, the stations are distributed over a significantly larger area than the most

significant observations of the Piemonte case, while at the same time, there are temporal correlations in the observed events, which can be seen from the columns in Fig. 7. The figures clearly show that several rainfall events of moderate strength occurred quite simultaneously within the shown period ranging from 22$^{\mathrm{nd}}$ of December 1994 to 15$^{\mathrm{th}}$ of February 1995. They all contributed to the floodings of river Meuse and river Rhine at the end of January 1995.

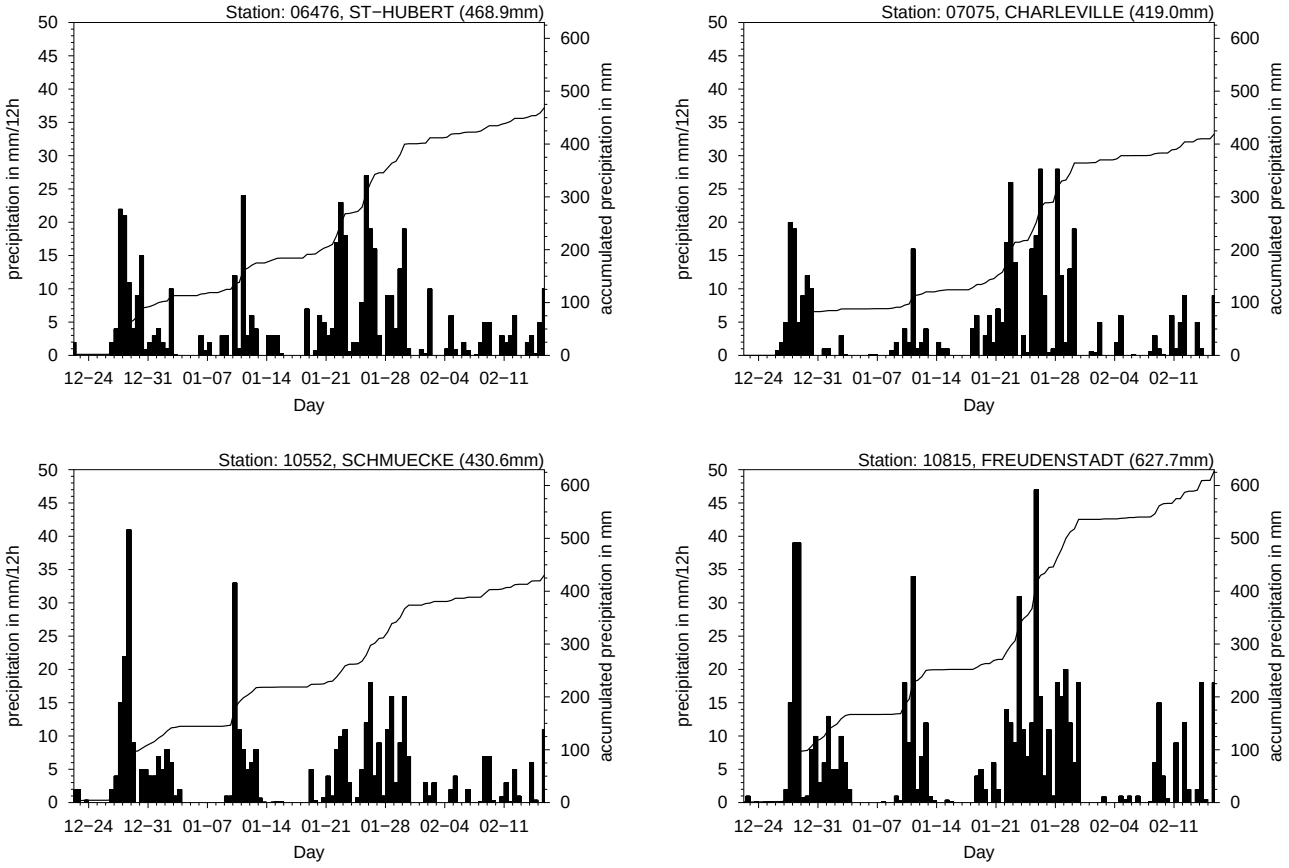

FIG. 7: Observed 12 hourly accumulated precipitation (columns, left ordinate) and pluviographs (curves, right ordinate) of four synoptic meteorological stations. St. Hubert (upper left) and Charleville (upper right) are located within the Meuse river catchment, Schmücke (lower left) and Freudenstadt (lower right) are located in or close to the river Rhine catchment. The depicted period comprises the days between 22$^{\mathrm{nd}}$ of December 1994 to 15$^{\mathrm{th}}$ of February 1995.

The rainfall events were due to a chain of troughs and frontal systems passing Europe from West, still under development, and persistently transporting humidity from the Atlantic eastwards. Furthermore, hydrological causes like snow melt also played a significant role for the flood to occur (Ulbrich and Fink, 1995).

The period selected for the hindcasts runs from 1$^{\mathrm{st}}$ of December 1994 to 2$^{\mathrm{nd}}$ of February 1995. A 3-day hindcast was launched for each day within this period, using the DMI-HIRLAM model as described in Sec. 2.

Data from precipitation analysis for this event was available for the most interesting part of the period, namely between 15$^{\mathrm{th}}$ of January and 2$^{\mathrm{nd}}$ of February 1995. In this case, the analysis is based on the synoptic rain gauges.

3.3 The Odra flooding in 1997

In July 1997, a quasi-stationary depression over Central Europe was the cause for strong precipitation in the area of Southern Poland, South-Eastern Germany and the Czech Republic. It affected the rivers Odra and Vistula. Dziadziusko and Krzymiski (1998) give a detailed description of the events related to the flooding.

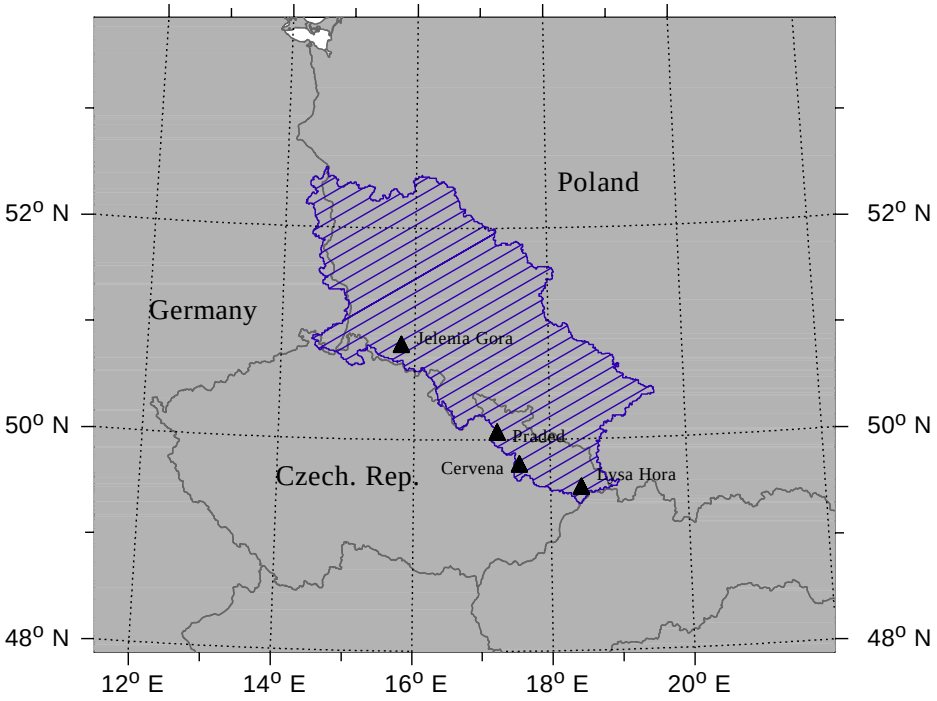

FIG. 8: Location of the four stations, which observed the largest rainfall amounts over the shown period. The river basin of the Po river is depicted by the hatched area.

The largest rainfall amounts were observed at the meteorological station Lysa Hora, which is located at the SE corner of the Odra river catchment (Fig. 8). It registered about 600 mm precipitation in the period from 5$^{\text{th}}$ of July to 10$^{\text{th}}$ of July (Fig. 9, lower left panel). Praded, which is located about 80 km NW of Lysa Hora, registered almost 500 mm during this period (Fig. 8 and Fig. 9 upper left panel). During a second major rainfall period after the 15$^{\text{th}}$ of July 1997 rainfall amounts of the order of 200 mm occurred over a larger area extending farther towards NW. This is indicated by the rain gauges at Jelenia Gora, Praded and Lysa Hora (Figs. 8 and 9).

The selected period for the hindcasts is between 25$^{\text{th}}$ of June and 31$^{\text{st}}$ of July 1997. The hindcasts were performed in the same way as in the other cases described above.

The precipitation analysis data was available for the first of the mentioned events, covering the period between 2$^{\text{nd}}$ and 15$^{\text{th}}$ of July 1997.

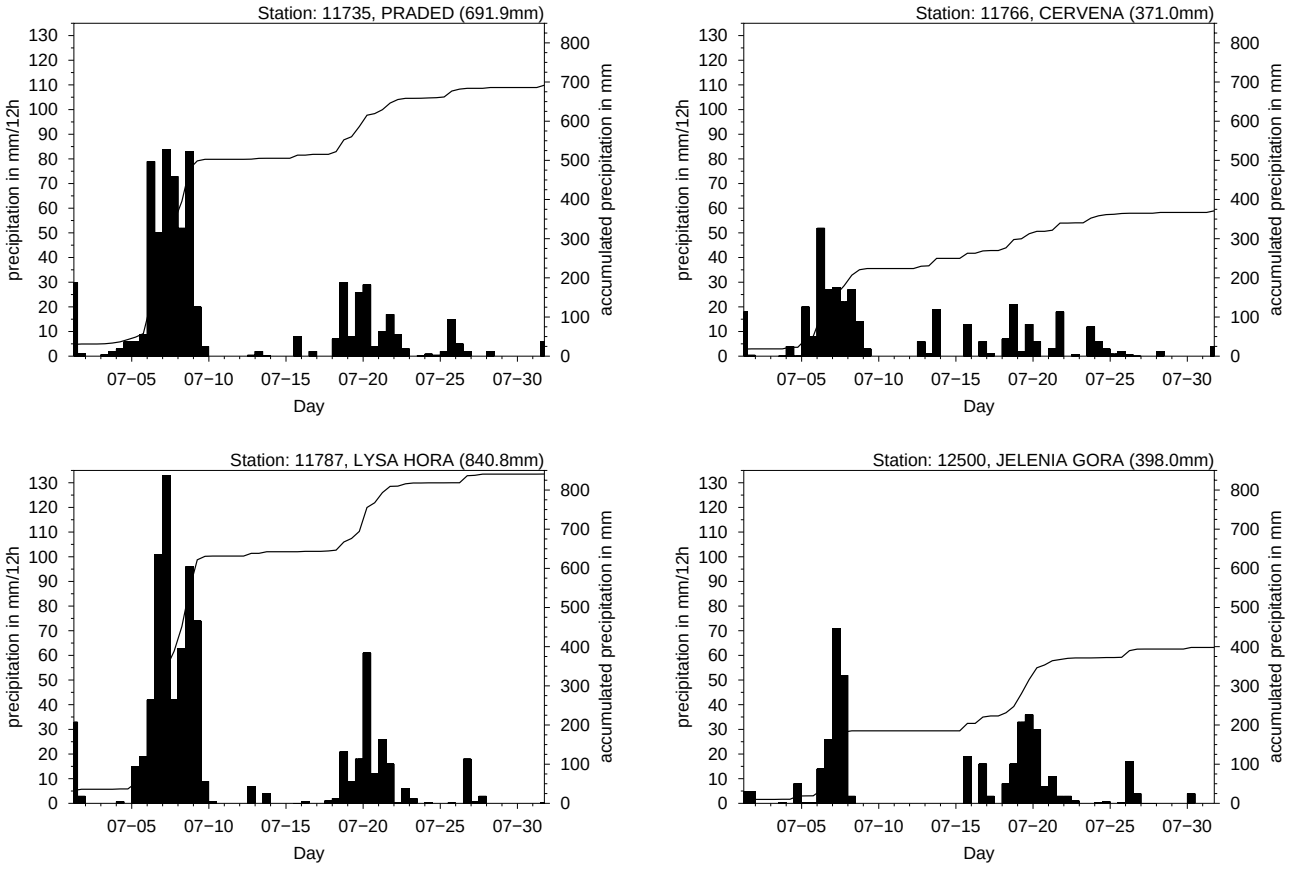

FIG. 9: Observed 12 hourly accumulated precipitation (columns, left ordinate) and pluviographs (curves, right ordinate) of the four synoptic meteorological stations Praded (upper left), Cervena (upper right), Lysa Hora (lower left) and Jelenia Gora (lower right), all located in the Odra river catchment. The depicted period comprises 1st to 31st of July 1997.

4 Results

The precipitation hindcasts for the three heavy rain events described in Section 3 were validated against precipitation field analysis from the Deutsche Wetterdienst. This validation was performed over those parts of the hindcasts periods, for which precipitation analysis data was available (see Section 3). Due to the different availability of rain gauge data, the analysis are based on different types of sources. In the Piemonte case, the analysis includes observations from synoptical and climatological rain gauges as well as other local measurements. The analysis for the Rhine/Meuse flood was performed by including synoptical stations only, and in the Odra case, synoptical and climatological rain gauges were applied.

The validation is performed over the respective river-catchments under consideration. Areal averaged precipitation amounts were determined for the hindcast fields as well as for the analyzed fields using areally weighted averaging in order to account for the different grid topologies of the DMI-HIRLAM grid and the grid, on which the precipitation analysis are based.

4.1 The Piemonte case 1994

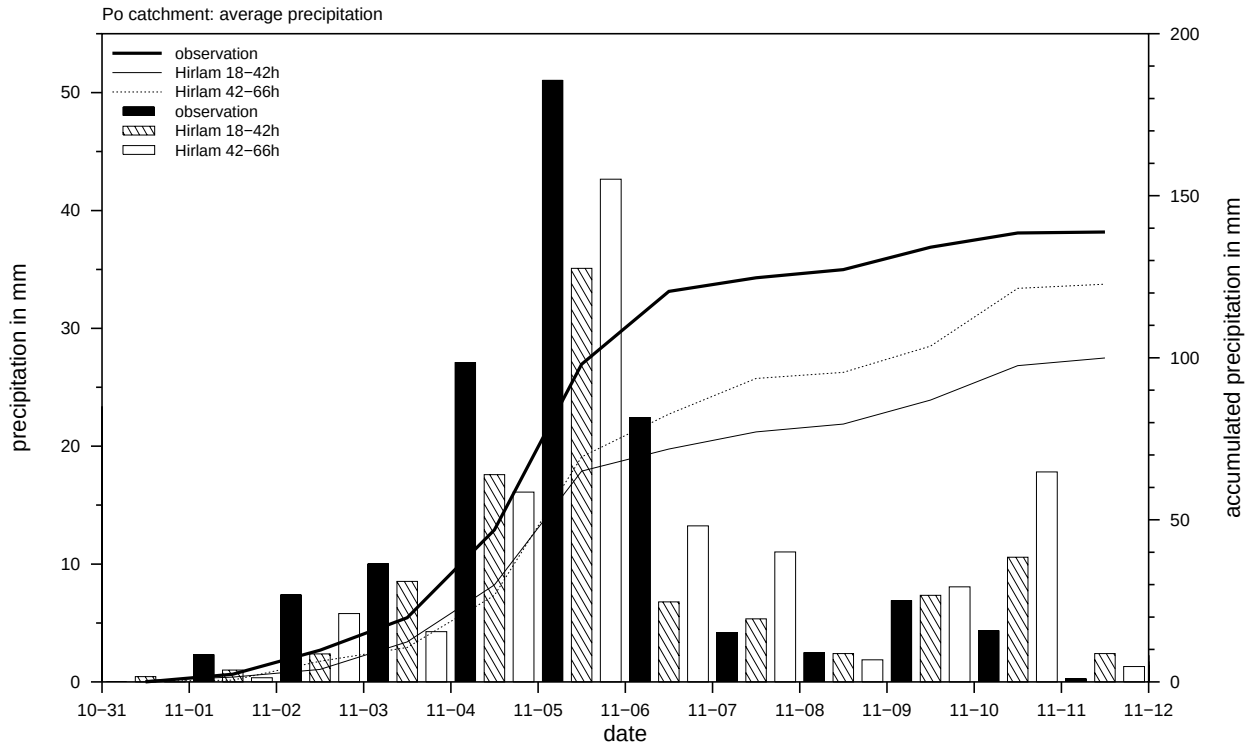

FIG. 10: Accumulated precipitation over 24 hours (columns and left axis) averaged over the Po river-catchment, from the DMI-HIRLAM hindcasts in the forecasting range 18–42h and 42–66h, and from precipitation analysis of synoptic and high resolution precipitation observations (observation). The curves denote the respective accumulations (axis to the right).

Figure 10 shows the results from the hindcasts within the period of the major precipitation event.

The peak rainfall event that occurred in this case is captured well by the hindcasts, and it is interesting that the hindcast for the longer lead time (42–66h) better predicts the rain volume observed at the 5$^{\text{th}}$ of November than the hindcast launched one day later (18–42h). When regarding the precipitation development up to the 7$^{\text{th}}$ of November, which can be regarded as the end of the major rainfall event (see the curves in Fig. 10), DMI-HIRLAM underestimates the accumulation of precipitated water by approximately 40% in the 18–42h prediction, and by about 28% only in the older 42–66h prediction.

Towards the end of the shown period, the hindcasts over-predict precipitation amounts, especially during the 10$^{\text{th}}$ of November (see columns for 11-10 in Fig. 10).

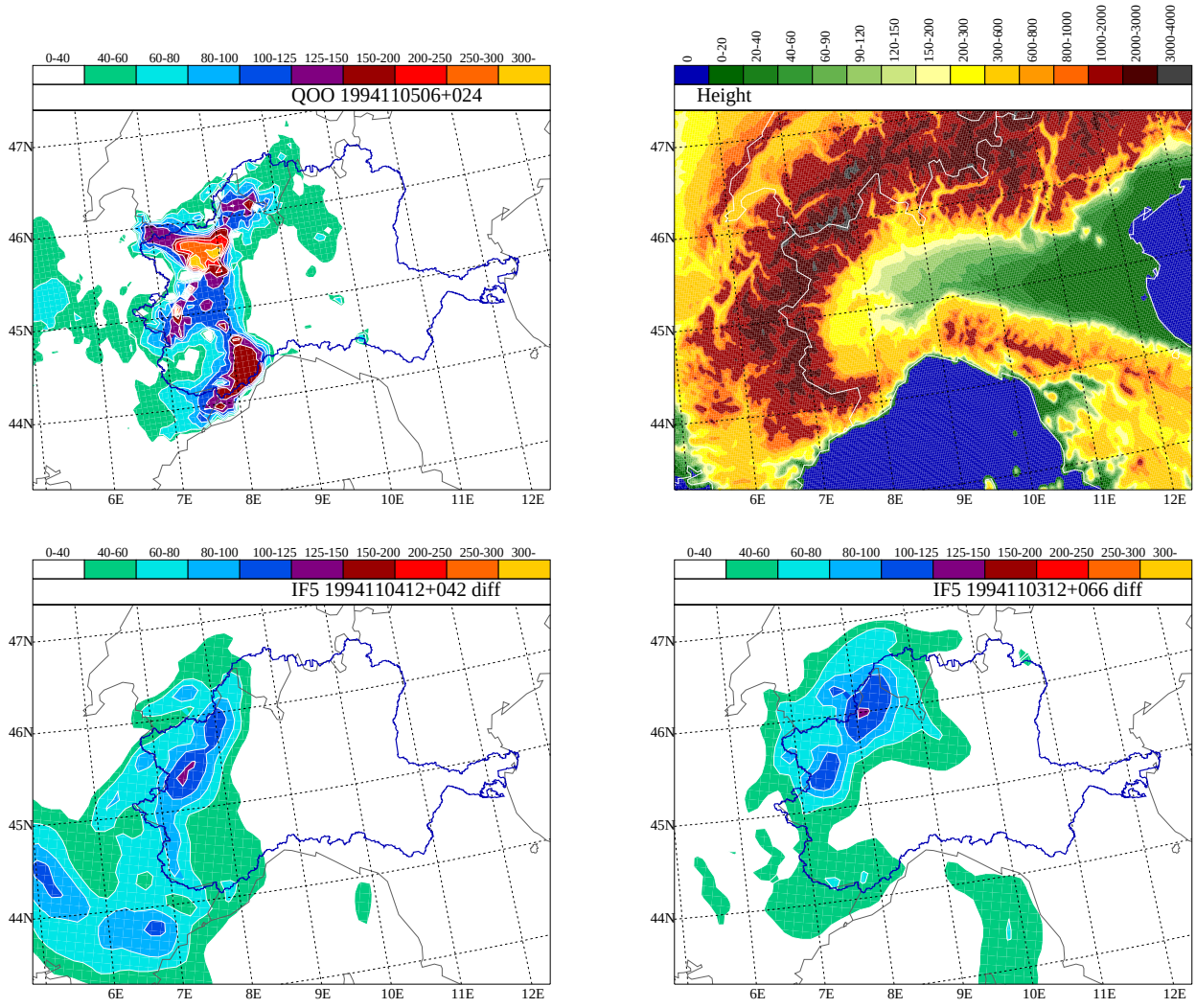

FIG. 11: 24 hour accumulated precipitation predicted over the Po river basin (dark blue) between 4 November and 5 November at 6 UTC, as analyzed from rain gauges (upper left), and as predicted by DMI-HIRLAM for a lead time of 42 hours (left lower panel) and 66 hours (right lower panels). The Orography of the region is shown in the upper right map.

In order to investigate, how the rainfall patterns were predicted by DMI-HIRLAM, Fig. 11 compares the analyzed observations of accumulated rainfall over a 24 hour period within the peak rainfall

event with respective model predictions. As the figures show, the location of the peak event is predicted quite well, placed in the North-western part of the Po river basin, south of the alpine chain. The secondary precipitation maximum over the southwestern part of the Po river catchment is, however, not predicted very well. The rainfall amounts in the 18–42h prediction from the 4$^{\mathrm{th}}$ of November on the other hand, over-predicts rainfall amounts over Southern France.

4.2 The Rhine/Meuse case 1995

The evolution of the average rainfall amounts over the river Rhine basin is given in Fig. 12. The 24-hourly precipitation amounts predicted by DMI-HIRLAM coincide very well with the observed amounts. It is striking that the 18–42h prediction and the 42–66h prediction perform almost equally well, and the estimates for the amount of precipitated water over the river basin only ly 6% below the observed amount. The course of the curves in Fig. 12 also show that DMI-HIRLAM slightly over-estimates precipitation amounts in the first part of the shown period, especially the elder prediction (dotted curve in Fig. 12). This is followed by a short period of underestimation during the 23$^{\mathrm{rd}}$ and 24$^{\mathrm{th}}$ of January. In the second half of the period, DMI-HIRLAM's estimations are very good.

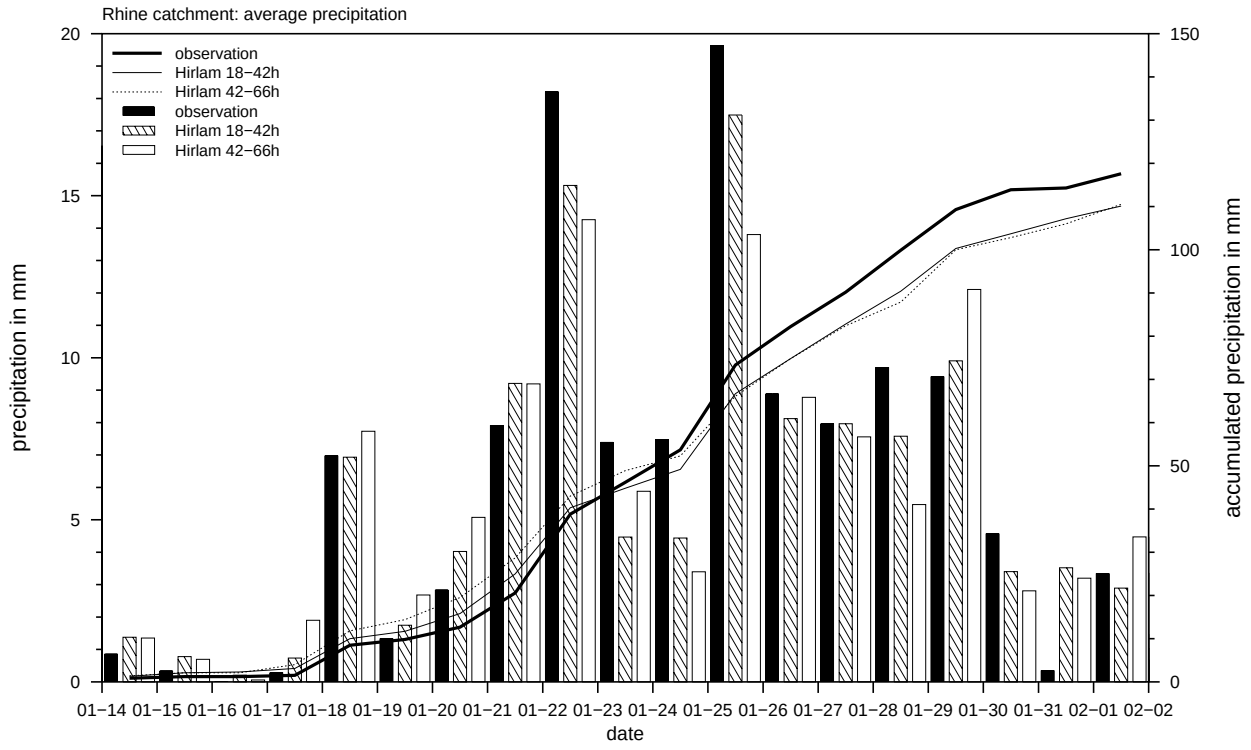

FIG. 12: Accumulated precipitation over 24 hours (columns and left axis) averaged over the river Rhine catchment, from the DMI-HIRLAM hindcasts in the forecasting range 18–42h and 42–66h, and from precipitation analysis of synoptic and high resolution precipitation observations (observation). The curves denote the respective accumulations (axis to the right).

The course of the hindcasts and the respective observation over the Meuse river basin are shown in Fig. 13. The columns show again a good temporal correlation to the observations. Like for the

river Rhine basin, DMI-HIRLAM slightly overestimates precipitation in the first part of the shown period, and underestimates it in the second part of the period. At the end of the period, the relative underestimation of precipitated water over the Meuse basin is about 13% for the 18–42h prediction, and about 23% for the 42–66h prediction (curves in Fig. 13).

As the catchment of the river Rhine is rather large, spatial distribution errors in the rainfall prediction do not show up as clearly as over the significantly smaller basin of the river Meuse. Therefore, the prediction errors over the Meuse basin affect the prediction to a larger extent than over the river Rhine basin. The performance of DMI-HIRLAM in predicting the rainfall patterns is roughly estimated for the 22$^{\mathrm{nd}}$ of January in Fig. 14. It should be noted that the rain gauge analyses is only available over land. As the figures show, both the longer and the shorter prediction capture the rainfall pattern well. The 42–66h prediction even indicates the location of the rainfall maximum over the Meuse basin very precisely. Comparison of the patterns also reveal the tendency of DMI-HIRLAM to over-predict small precipitation amounts while tending to underestimate the larger amounts.

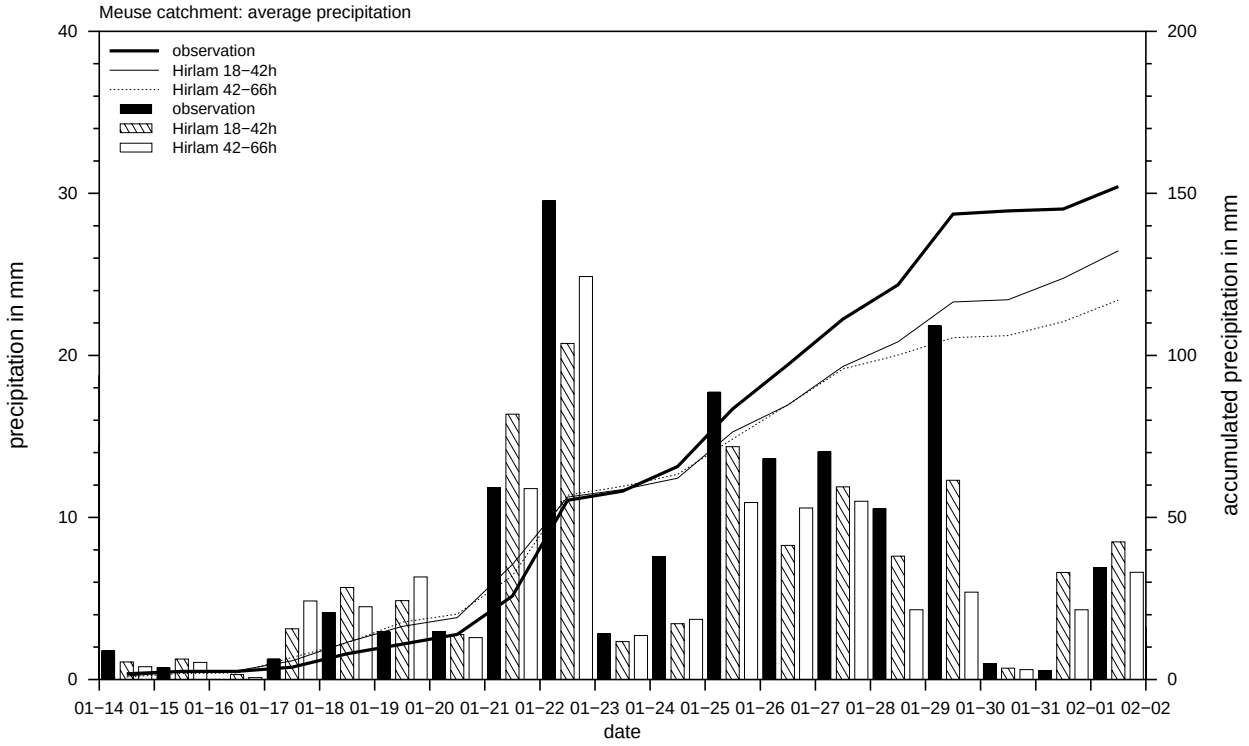

FIG. 13: Accumulated precipitation over 24 hours (columns and left axis) averaged over the Meuse river-catchment, from the DMI-HIRLAM hindcasts in the forecasting range 18–42h and 42–66h, and from precipitation analysis of synoptic and high resolution precipitation observations (observation). The curves denote the respective accumulations (axis to the right).

Unfortunately, the rainfall pattern is, however, not always predicted so well as for the 22$^{\mathrm{nd}}$ of January. An example for this occurs for the 29$^{\mathrm{th}}$ of January, where DMI-HIRLAM underestimated the rainfall over the Meuse basin (see Fig. 13). The 24 hour accumulated precipitation fields are shown in Fig. 15. In this case, the 42–66h prediction fails to capture the development leading to the observed rainfall pattern. The 18–42h prediction, on the other hand, reveals a significantly improved

pattern. It is, however, weak and does not show the small-scale rainfall peaks from the analysis over the Meuse basin, which shows more than 40 mm of local precipitation.

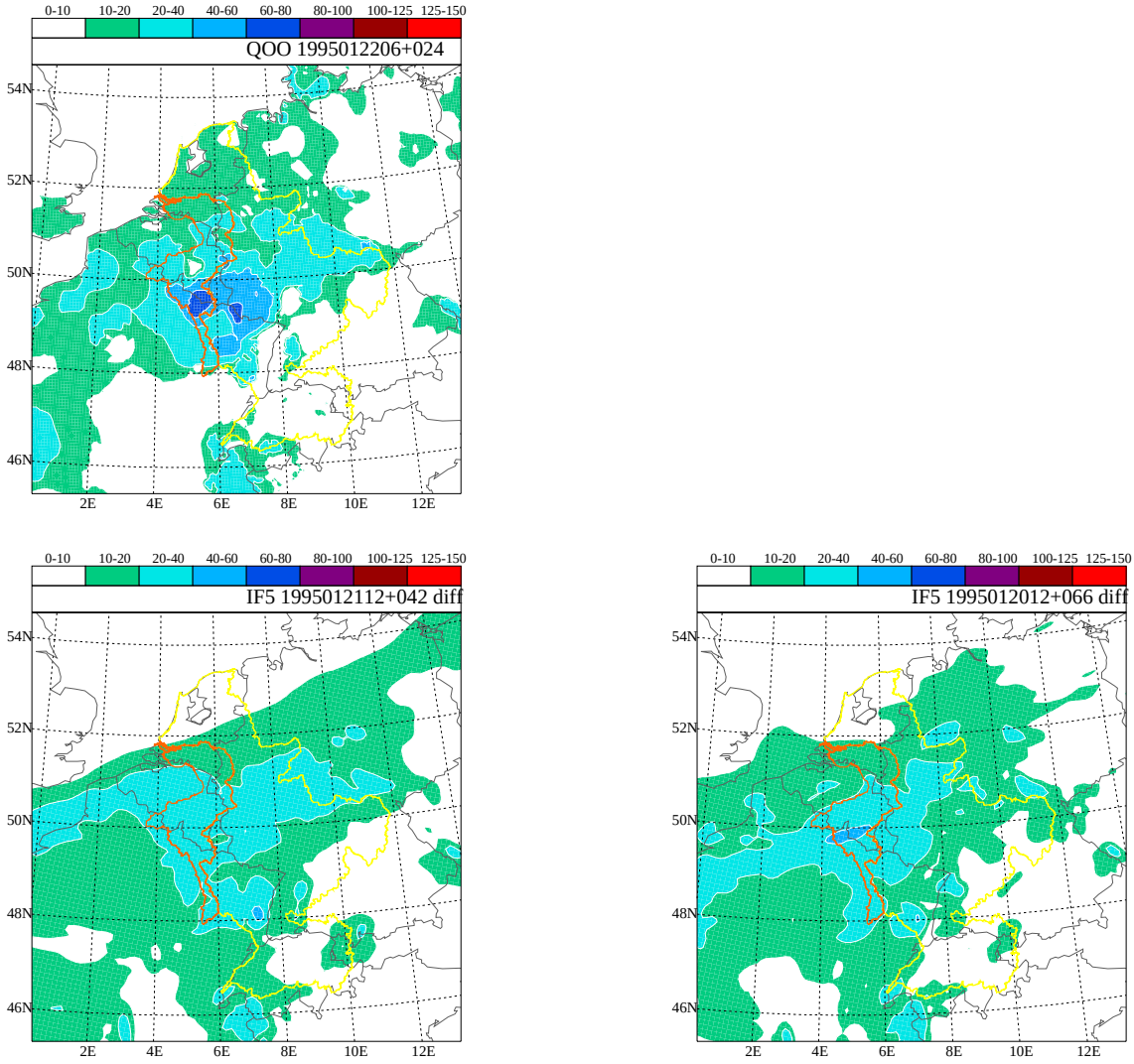

FIG. 14: 24 hour accumulated precipitation fields for the 22nd of January 1995. The river basins of the river Rhine and Meuse are outlined in yellow and red, respectively. Analyzed rain gauges are shown in the upper left panel, and predicted fields by DMI-HIRLAM are shown below for the prediction range 18–42h (lower left) and for 42–66h (lower right).

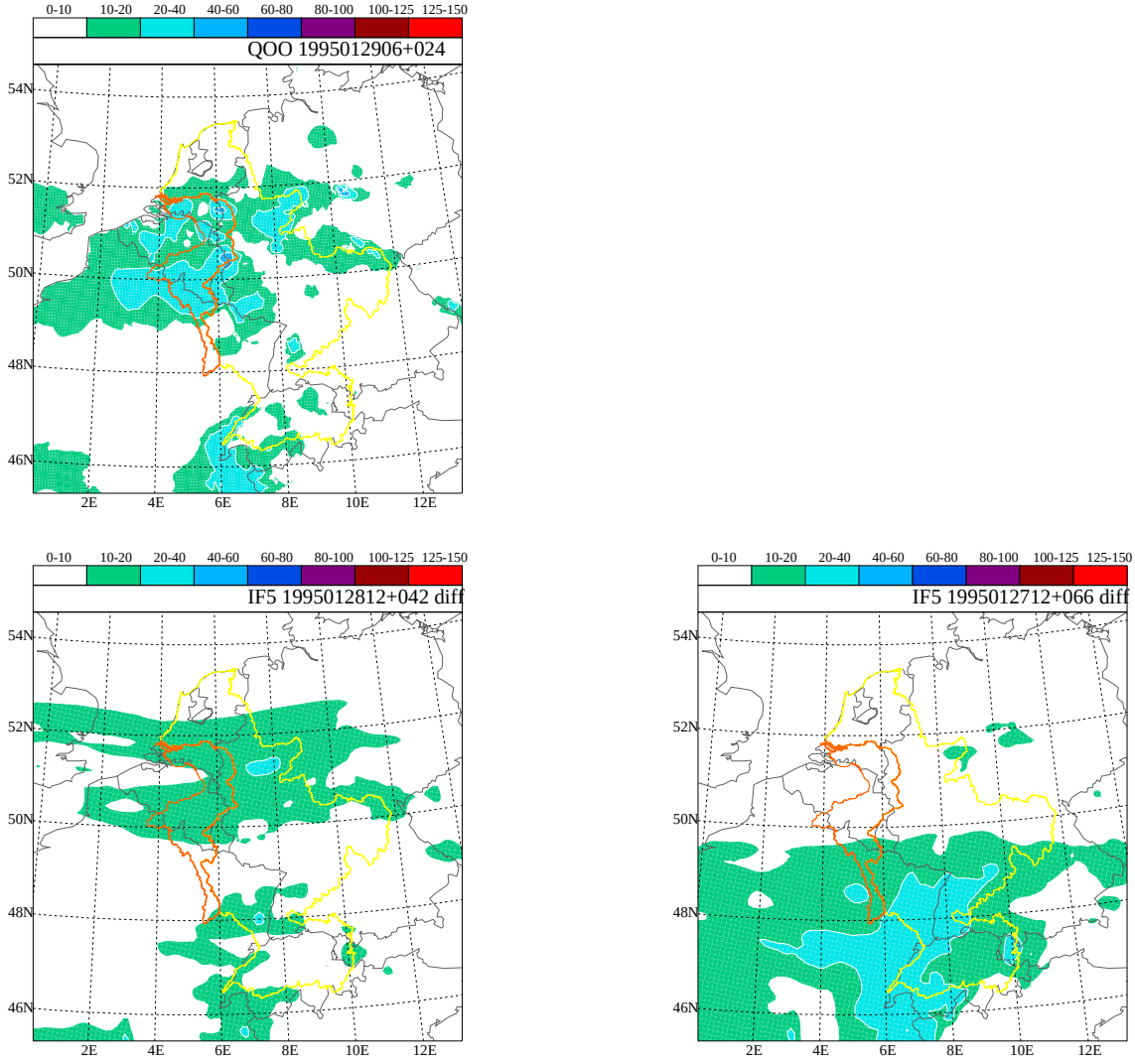

FIG. 15: 24 hour accumulated precipitation fields for the 29$^{\text{th}}$ of January 1995. The river basins of the river Rhine and Meuse are outlined in yellow and red, respectively. Analyzed rain gauges are shown in the upper left panel, and predicted fields by DMI-HIRLAM are shown below for the prediction range 18–42h (lower left) and for 42–66h (lower right).

4.3 The Odra case 1997

The results from the period 1st to 15th of July 1997, which cover the first major rainfall event of this case, are given in Fig. 16. The significant under-prediction in the hindcasts is very striking in this case. Even though the temporal correlation between hindcasts and observation is very good, all hindcasts systematically underestimate the development of the depression, but there is no significant deterioration in the longer prediction range, which indicates that the cause for the differences is already present at an early stage of the hindcast. This may even indicate that significant uncertainties where already present in the initial condition of the hindcasts.

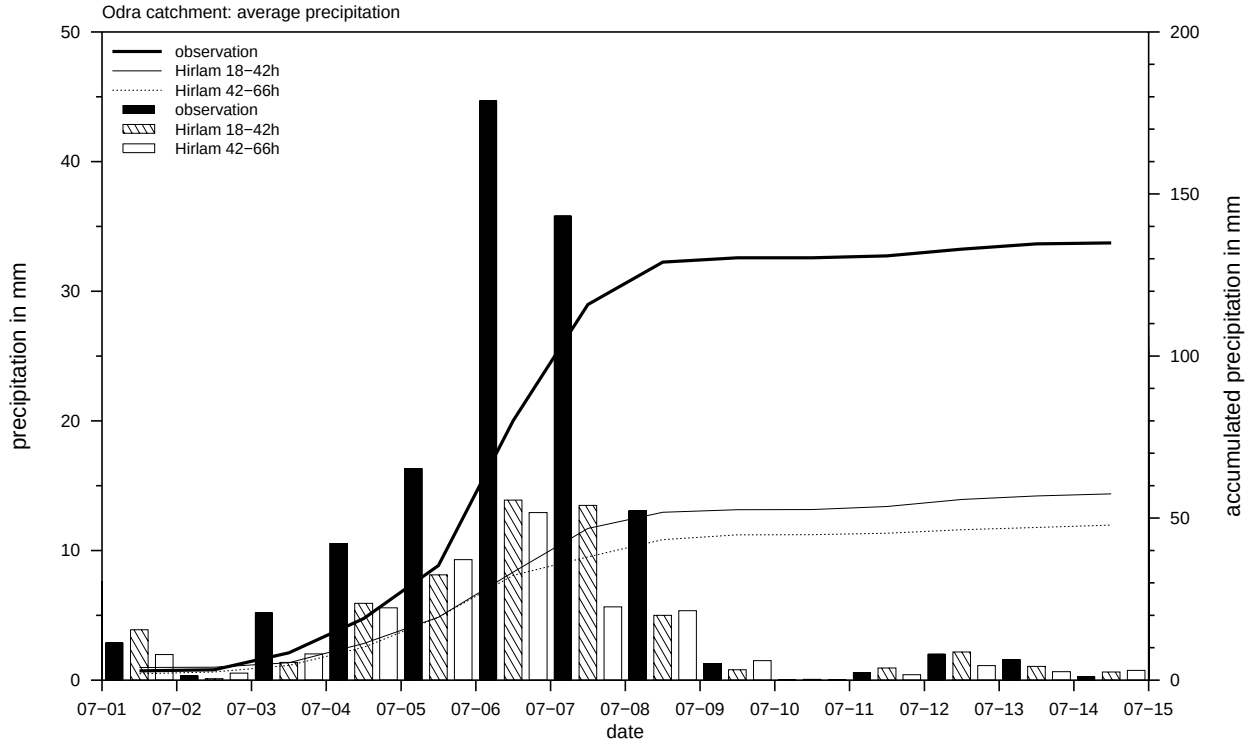

FIG. 16: Accumulated precipitation of the last 24 hours (columns and left axis) averaged over the Odra river-catchment, from the DMI-HIRLAM hindcasts in the forecasting range 18–42h and 42–66h, and from precipitation analysis of synoptic and high resolution precipitation observations (observation). The curves denote the respective accumulations (axis to the right).

The relative deviation of the accumulated rainfall over the Odra river basin at the end of the event are about -56% for the 42–66h prediction, and about -65% for the 18–42h prediction. The comparison of the rain areas from the 5th, 6th and 7th of July, respectively, indicate that the dynamical development of the depression was underestimated (Figs. 18, 19 and 20). This is confirmed by the fact that the relation between convective and stratiform rainfall in the model is larger than one, i. e. the major part of the rainfall amount in the model is convective for this case, which can be expected. This is true for both the 18–42h prediction (Fig. 17) and for the 42–66h prediction (not shown).

In addition to the weak development, DMI-HIRLAM places the location of the major precipitation during the first three days shown in Figs. 18 to 20 too far eastwards. This led to the effect that

the model precipitation, instead of falling within the Odra catchment, was released east of the river basin. This case clearly demonstrates that a minor change in the location of the peak precipitation can cause the estimation of the volume of water received by a river catchment to change significantly. This can subsequently lead to an erroneous water level prediction when applied in a hydrological water runoff model.

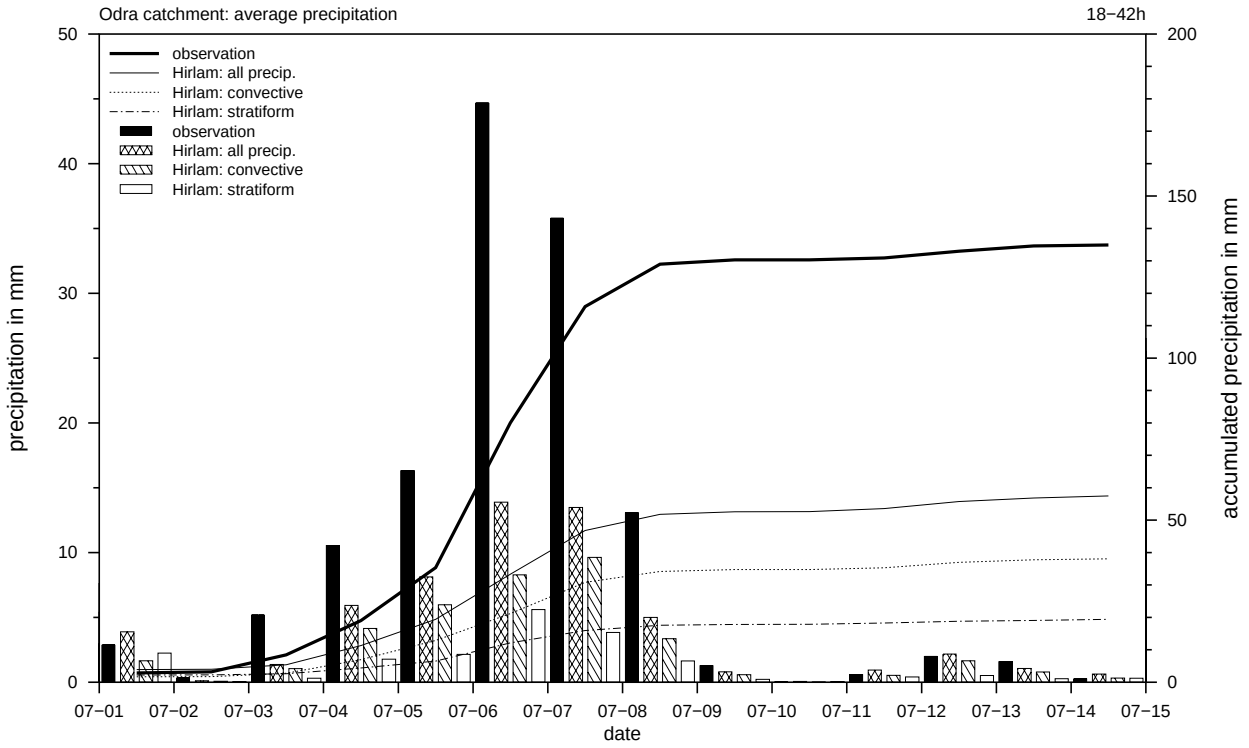

FIG. 17: Accumulated precipitation of the last 24 hours (columns and left axis) averaged over the Odra river-catchment, from the DMI-HIRLAM hindcasts in the forecasting range 18–42h. The hatched and outlined columns depict the model overall precipitation as well as its separation into convective and stratiform rain. The precipitation analysis of synoptic and high resolution precipitation observations is depicted by the black columns (observation). The curves denote the respective accumulations (axis to the right).

In contrast to the prediction errors in the forecast range beyond 18 hours, the predicted rainfall during the first 24 hours indicate that the model performed better in the short range. Even though not fully consistent in time range, Fig. 21 shows the predicted rainfall of the first 24 hours. The prediction from the 5^{th} of July shows a rain area displaced towards the East (compare upper left panel of Figs. 21 and 18). The predictions for the following days tend to perform better. The model is capable of capturing the main features of the observed rain areas, the dynamic development, however, is still insufficient (compare panels of Figs. 21 and 18, respectively). It seems that the latter is the cause for the deterioration of the rainfall prediction beyond the first prediction day.

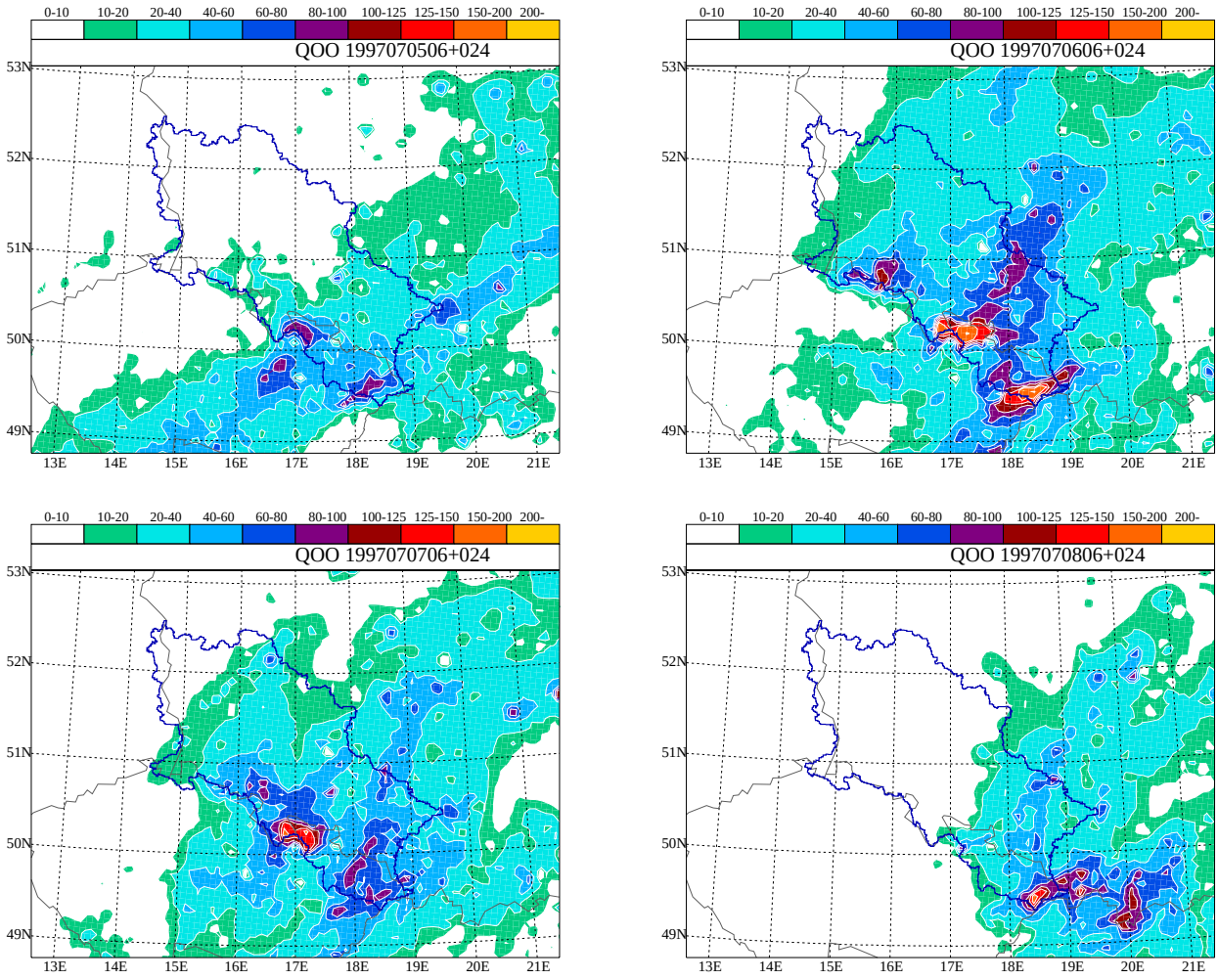

FIG. 18: Analyzes of rain gauge data for the 5^{th} (upper left), the 6^{th} (upper right), 7^{th} (lower left) and 8^{th} of July 1997 over the Odra river basin (dark blue).

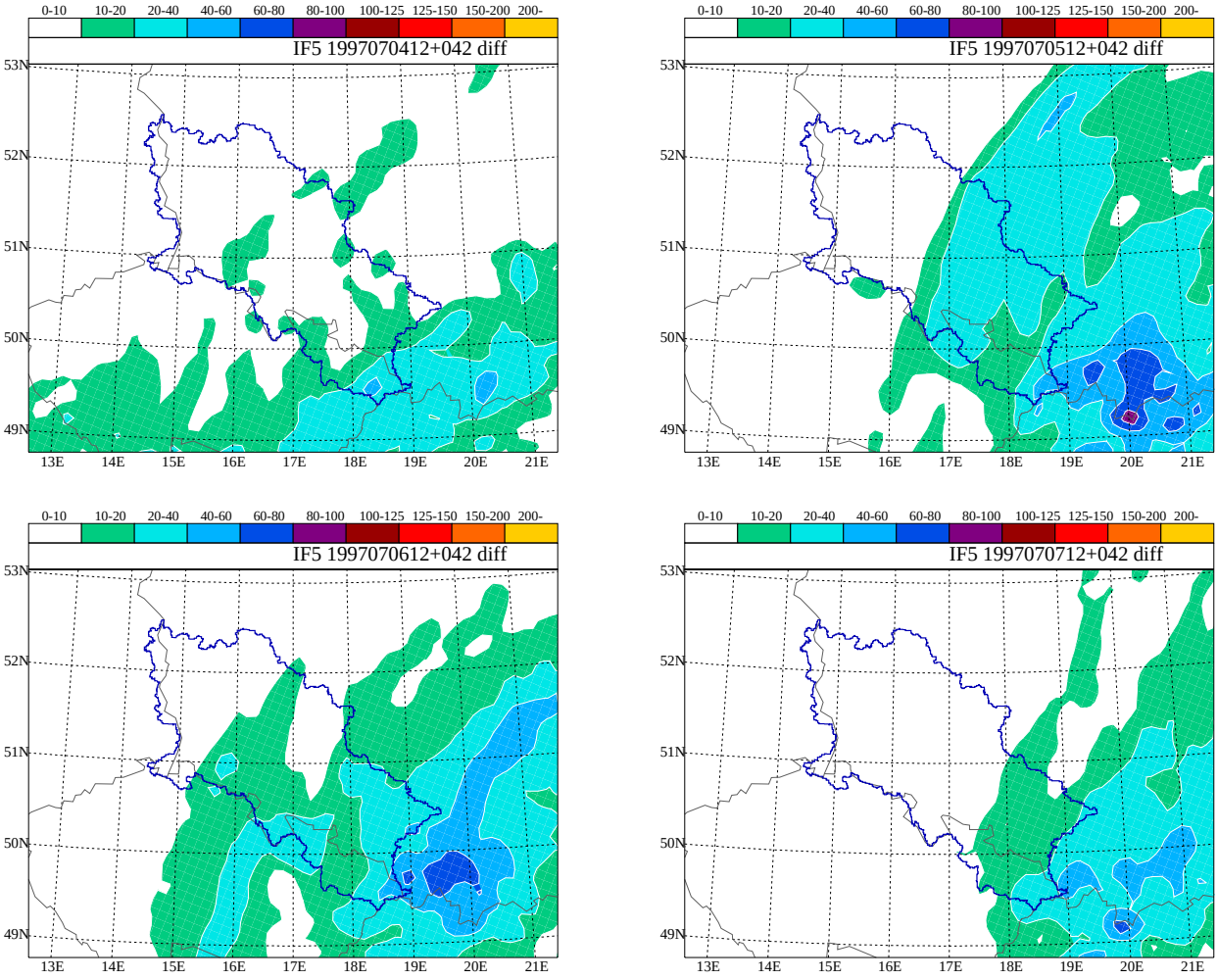

FIG. 19: Predicted rainfall of 18–42 hours lead time for the 5^{th} (upper left), the 6^{th} (upper right), 7^{th} (lower left) and 8^{th} of July 1997 over the Odra river basin (dark blue).

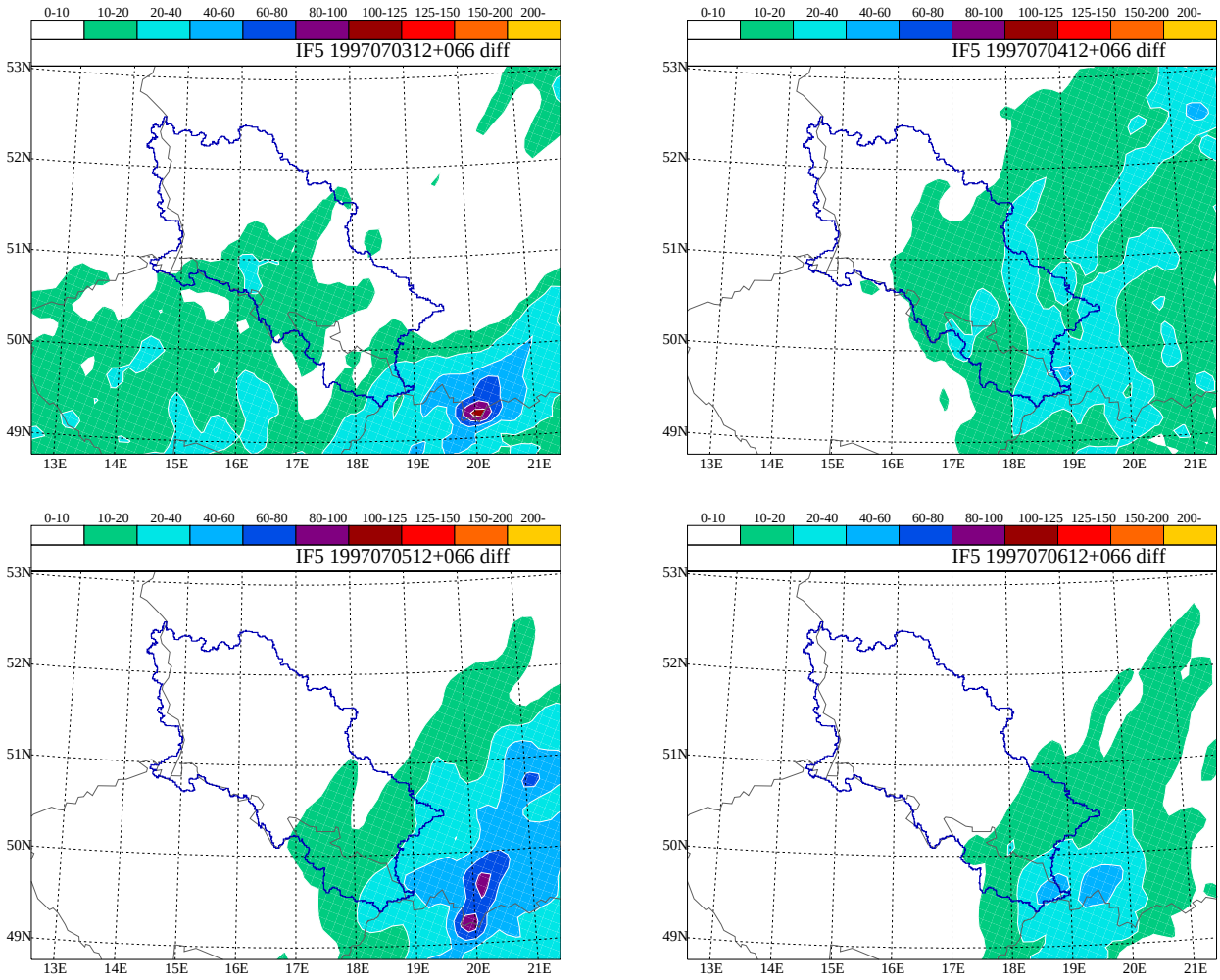

FIG. 20: Predicted rainfall of 42–66 hours lead time for the 5^{th} (upper left), the 6^{th} (upper right), 7^{th} (lower left) and 8^{th} of July 1997 over the Odra river basin (dark blue).

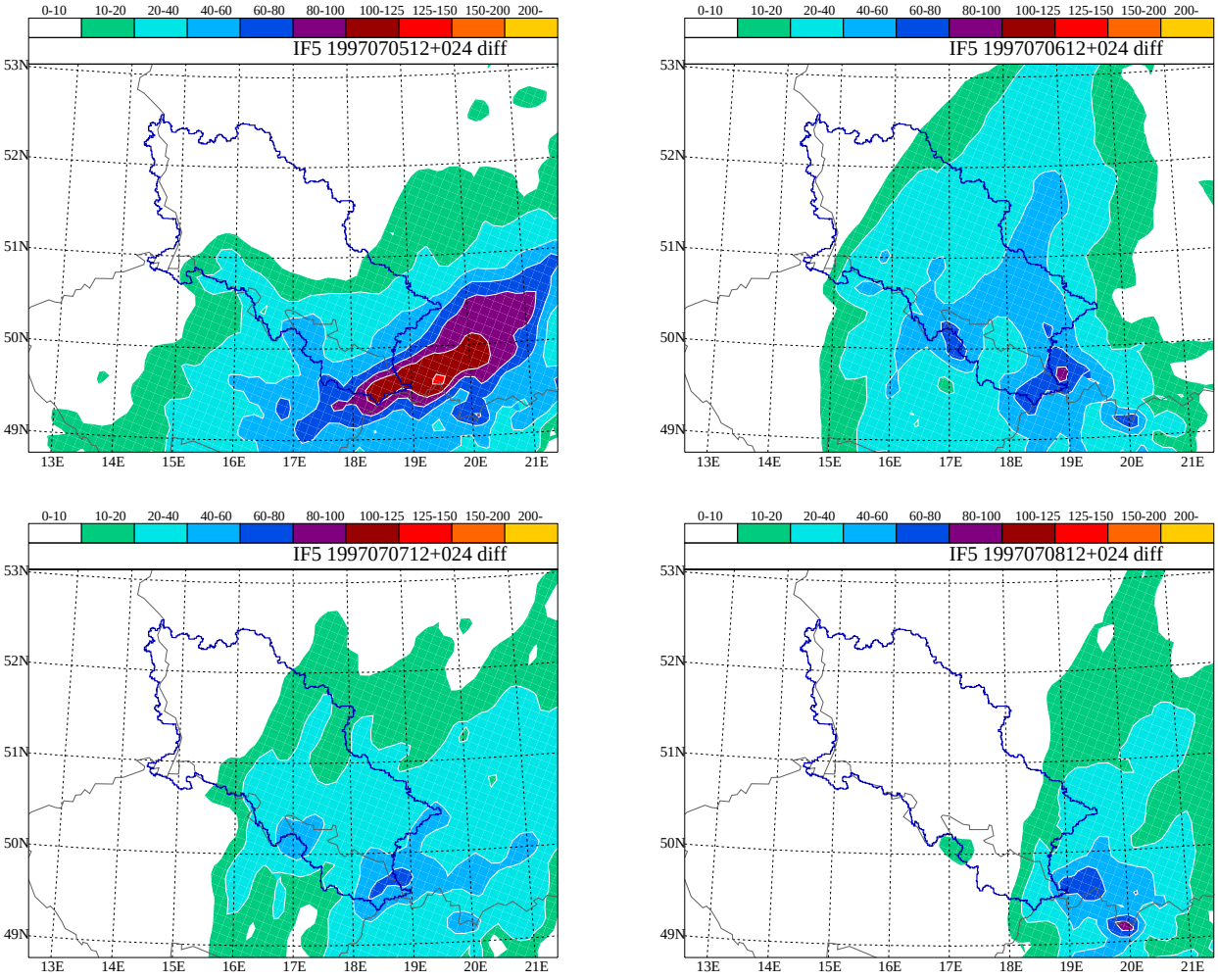

FIG. 21: Predicted rainfall of the first 24 hours lead time for the 5^{th} (upper left), the 6^{th} (upper right), 7^{th} (lower left) and 8^{th} of July 1997 over the Odra river basin (dark blue).

5 Conclusions and Outlook

Hindcasts with the DMI-HIRLAM model have been performed for three historical heavy rain events. The precipitation fields from these hindcasts have been compared to field analysis data based on rain gauge observations. The comparisons were concentrated on the respective river catchments affected by the rainfall.

The three historical events cover one summer case and two cases occurring during fall and winter, respectively. The cases are different with respect to synoptic pattern, location, precipitation triggering and type, as well as the spatio-temporal extension of the rainfall leading to a river flooding.

The performance of DMI-HIRLAM is quite different in the three cases. The model captures the temporal onset of the rainfall events well in the Piemonte case (November 1994), where orographic forcing plays a significant role, but also in the Rhine/Meuse case (January 1995), where a chain of troughs under dynamic development were invloved. In the Odra case, a weak dynamic development in the model connected with a spatial displacement of the rain area just outside the considered river basin leads to a significant under-prediction of the precipitation volume over the river basin. This happens already beyond the prediction range of 18 hours,

The hindcasts of the Rhine/Meuse case reveal to be of a very good quality when regarding the large river Rhine basin. Even in the forecast range between 42 hours and 66 hours the predicted precipitation amounts coincide very well with the observed amounts. Except for some days of the hindcasts for the Piemonte event the hindcast quality over the small river basins decreases with lead time, as one usually expects.

DMI-HIRLAM still has, in the version used for the hindcasts, a negative bias in predicting large amounts of rainfall. This leads to the area total of precipitated water for a small river basin to be under-predicted typically by 20% to 40%. Additional errors in the location of the rain area of a certain threshold can increase this further. Even though the causes for such displacements of the rain area have not been investigated in this work, it may be concluded that the displacement is not happening systematically.

On the other hand, DMI-HIRLAM tends to overestimate small precipitation amounts (e. g. Nielsen and Amstrup, 2002). Future versions of the convection scheme will include improvements to these systematic errors.

Especially the hindcasts of the Odra case suffer from errors already at an early stage of the forecast range. One cause for the errors may be due to uncertainties in the analysis of the initial state of the model simulations. An advanced data assimilation system, which includes new observation types like satellite based measurements can help to improve the precipitation predictions. As an example there is indication for that the exploitation of zenit total delay (ZTD) measurements from GPS satellites helps to improve the prediction of large rainfall amounts in the very short range (Vedel, 2002 personal communication).

It becomes clear from the above results that especially when regarding areas like small river basins, forecast errors of location, even though not large, may lead to significant errors over the area under consideration. In addition, wrong estimation of dynamical development by the model can deteri-

orate the situation. These errors are not solely of systematic nature and even small uncertainties in the initial state as well as model intrinsic uncertainties can lead to significant deviations within the forecast range. Such errors may be addressed by an ensemble approach, which is capable of capturing the consequences of these uncertainties. An aspect of the ongoing work is therefore an attempt to design an ensemble of HIRLAM simulations, which can help to improve the random errors. This approach is to be based on the ensemble prediction system (EPS) of the ECMWF, where a small subset of "significant members" are selected for simulation using DMI-HIRLAM in order to account for uncertainties in the representation of the initial state. This "mini ensemble" may then be supplemented with further simulations using different model configurations like for example the variation of parameterization of convection and condensation processes.

Acknowledgments

This work is part of the EC funded project "An European Flood Forecasting System" (EFFS), contract No. EVG1-CT-1999-00011.

The Dipartimento di Scienze della Terra e Geologico Ambientali provided the river catchment data of the Po basin, and Riza, WL Delft Hydraulics and the JRC provided river catchment data of the Rhine and the Meuse basin. The precipitation analysis on the LM-grid were kindly provided by Deutscher Wetterdienst (DWD), who also included rainfall data from the Mesoscale Alpine Programme (MAP, 2002) in the rainfall analyses for the Piemonte 1994 event.

References

Buzzi, A., Cacciamani, C., Paccagnella, T., Patruno, P., Tartaglione, N, 1995: Preliminary meteorological analysis of the Piedmont flood of November 1994. *MAP Newsletter*, **2**, 2–6.

Cuxart, J., Bougeault, P., and Redelsperger, j.-L., 2000: Turbulence closure for a non-hydrostatic model. *Q. J. R. Meteor. Soc.*, **126**, 1–30.

Doms, G., Schättler, U., 1999: The non-hydrostatic limited-area model LM (Lokal-Modell) of DWD. Part I: Scientific documentation. Available from Deutscher Wetterdienst, Geschäftsbereich Forschung und Entwicklung, Postfach 100465, 63004 Offenbach, Germany.

Dziadziusko, Z. and Krzymiski, W., 1998: Meteorological Origin of the Flood and its Hydrological Effects in the Odra and Vistula Rivers (Summary). *Deutsche Hydrogr. Zeitschr.*, **50**, 2/3, 259–260.

Fink, A., Ulbrich, U., Engel, H., 1995: Aspects of the January 1995 flood in Germany. *Weather*, **51-2**, 34–39.

Källén, E. (ed.), 1996: *HIRLAM Documentation Manual system 2.5*. Available from the Swedish Meteorological and Hydrological Institute (SMHI) Norrköping, Sweden.

MAP, 2002: The MAP Data Centre. MeteoSwiss, Krähbühlstr. 58, CH-8044 Zürich.

Meijgaard, E. van and Jilderda, R., 1995: The Meuse flood in January 1995. *Weather*, **51-2**, 39–45.

Nielsen, N.W., Amstrup, B., 2002: Kvartalsrapport for 1. kvartal 2002. *DMI internal report*, **02-05**. Available from Danish Meteorological Institute.

Sarvijärvi, H., 1990: Fast Radiation parameterization schemes for Mesoscale and Short-Range Forecast Models. *J. Appl. Meteor.*, **29**, 437–447.

Sass, B.H., 1997: Reduction of numerical noise connected to the parameterization of cloud and condensation processes in the HIRLAM model. *HIRLAM Newsletter*, **29**, 37–45. Available at SMHI.

Sass, B.H., Nielsen, N.W., Jørgensen, J.U., Amstrup, B., Kmit, M., 2000: The operational DMI-HIRLAM system. *DMI Tech. Rep.*, **00-26**. Available from DMI.

Sattler, K.; 1999: New high resolution physiographic data and climate generation for the HIRLAM forecasting system. *DMI Tech. Rep.*, **99-11**. 38pp.

Ulbrich, U. and Fink, A., 1995: The January 1995 Flood in Germany: Meteorological Versus Hydrological Causes. *Phys. Chem. Earth*, **20**, 439–444.

DANISH METEOROLOGICAL INSTITUTE

Scientific Reports

Scientific reports from the Danish Meteorological Institute cover a variety of geophysical fields, i.e. meteorology (including climatology), oceanography, subjects on air and sea pollution, geomagnetism, solar-terrestrial physics, and physics of the middle and upper atmosphere.

Reports in the series within the last five years:

No. 97-1
E. Friis Christensen og C. Skøtt: Contributions from the International Science Team. The Ørsted Mission - a pre-launch compendium

No. 97-2
Alix Rasmussen, Sissi Kiilsholm, Jens Havskov Sørensen, Ib Steen Mikkelsen: Analysis of tropospheric ozone measurements in Greenland: Contract No. EV5V-CT93-0318 (DG 12 DTEE):
DMI's contribution to CEC Final Report Arctic Trophospheric Ozone Chemistry ARCTOC

No. 97-3
Peter Thejll: A search for effects of external events on terrestrial atmospheric pressure: cosmic rays

No. 97-4
Peter Thejll: A search for effects of external events on terrestrial atmospheric pressure: sector boundary crossings

No. 97-5
Knud Lassen: Twentieth century retreat of sea-ice in the Greenland Sea

No. 98-1
Niels Woetman Nielsen, Bjarne Amstrup, Jess U. Jørgensen: HIRLAM 2.5 parallel tests at DMI: sensitivity to type of schemes for turbulence, moist processes and advection

No. 98-2
Per Høeg, Georg Bergeton Larsen, Hans-Henrik Benzon, Stig Syndergaard, Mette Dahl Mortensen: The GPSOS project Algorithm functional design and analysis of ionosphere, stratosphere and troposphere observations

No. 98-3
Mette Dahl Mortensen, Per Høeg: Satellite atmosphere profiling retrieval in a nonlinear troposphere Previously entitled: Limitations induced by Multipath

No. 98-4
Mette Dahl Mortensen, Per Høeg: Resolution properties in atmospheric profiling with GPS

No. 98-5
R.S. Gill and M. K. Rosengren: Evaluation of the Radarsat imagery for the operational mapping of sea ice around Greenland in 1997

No. 98-6
R.S. Gill, H.H. Valeur, P. Nielsen and K.Q. Hansen: Using ERS SAR images in the operational mapping of sea ice in the Greenland waters: final report for ESA-ESRIN's: pilot projekt no. PP2.PP2.DK2 and 2nd announcement of opportunity for the exploitation of ERS data projekt No. AO2..DK 102

No. 98-7
Per Høeg et al.: GPS Atmosphere profiling methods and error assessments

No. 98-8
H. Svensmark, N. Woetmann Nielsen and A.M. Sempreviva: Large scale soft and hard turbulent states of the atmosphere

No. 98-9
Philippe Lopez, Eigil Kaas and Annette Guldberg: The full particle-in-cell advection scheme in spherical geometry

No. 98-10
H. Svensmark: Influence of cosmic rays on earth's climate

No. 98-11
Peter Thejll and Henrik Svensmark: Notes on the method of normalized multivariate regression

No. 98-12
K. Lassen: Extent of sea ice in the Greenland Sea 1877-1997: an extension of DMI Scientific Report 97-5

No. 98-13
Niels Larsen, Alberto Adriani and Guido DiDonfrancesco: Microphysical analysis of polar stratospheric clouds observed by lidar at McMurdo, Antarctica

No.98-14
Mette Dahl Mortensen: The back-propagation method for inversion of radio occultation data

No. 98-15
Xiang-Yu Huang: Variational analysis using spatial filters

No. 99-1
Henrik Feddersen: Project on prediction of climate variations on seasonel to interannual timescales (PROVOST) EU contract ENVA4-CT95-0109: DMI contribution to the final report:Statistical analysis and post-processing of uncoupled PROVOST simulations

No. 99-2
Wilhelm May: A time-slice experiment with the ECHAM4 A-GCM at high resolution: the experimental design and the assessment of climate change as compared to a greenhouse gas experiment with ECHAM4/OPYC at low resolution

No. 99-3
Niels Larsen et al.: European stratospheric monitoring stations in the Artic II: CEC Environment and Climate Programme Contract ENV4-CT95-0136. DMI Contributions to the project

No. 99-4
Alexander Baklanov: Parameterisation of the deposition processes and radioactive decay: a review and some preliminary results with the DERMA model

No. 99-5
Mette Dahl Mortensen: Non-linear high resolution inversion of radio occultation data

No. 99-6
Stig Syndergaard: Retrieval analysis and methodologies in atmospheric limb sounding using the GNSS radio occultation technique

No. 99-7
Jun She, Jacob Woge Nielsen: Operational wave forecasts over the Baltic and North Sea

No. 99-8
Henrik Feddersen: Monthly temperature forecasts for Denmark - statistical or dynamical?

No. 99-9
P. Thejll, K. Lassen: Solar forcing of the Northern hemisphere air temperature: new data

No. 99-10
Torben Stockflet Jørgensen, Aksel Walløe Hansen: Comment on "Variation of cosmic ray flux and global coverage - a missing link in solar-climate relationships" by Henrik Svensmark and Eigil Friis-Christensen

No. 99-11
Mette Dahl Meincke: Inversion methods for atmospheric profiling with GPS occultations

No. 99-12
Hans-Henrik Benzon; Laust Olsen; Per Høeg: Simulations of current density measurements with a Faraday Current Meter and a magnetometer

No. 00-01
Per Høeg; G. Leppelmeier: ACE - Atmosphere Climate Experiment

No. 00-02
Per Høeg: FACE-IT: Field-Aligned Current Experiment in the Ionosphere and Thermosphere

No. 00-03
Allan Gross: Surface ozone and tropospheric chemistry with applications to regional air quality modeling. PhD thesis

No. 00-04
Henrik Vedel: Conversion of WGS84 geometric heights to NWP model HIRLAM geopotential heights

No. 00-05
Jérôme Chenevez: Advection experiments with DMI-Hirlam-Tracer

No. 00-06
Niels Larsen: Polar stratospheric clouds microphysical and optical models

No. 00-07
Alix Rasmussen: "Uncertainty of meteorological parameters from DMI-HIRLAM"

No. 00-08
A.L. Morozova: Solar activity and Earth's weather. Effect of the forced atmospheric transparency changes on the troposphere temperature profile studied with atmospheric models

No. 00-09
Niels Larsen, Bjørn M. Knudsen, Michael Gauss, Giovanni Pitari: Effects from high-speed civil traffic aircraft emissions on polar stratospheric clouds

No. 00-10
Søren Andersen: Evaluation of SSM/I sea ice algorithms for use in the SAF on ocean and sea ice, July 2000

No. 00-11
Claus Petersen, Niels Woetmann Nielsen: Diagnosis of visibility in DMI-HIRLAM

No. 00-12
Erik Buch: A monograph on the physical oceanography of the Greenland waters

No. 00-13
M. Steffensen: Stability indices as indicators of lightning and thunder

No. 00-14
Bjarne Amstrup, Kristian S. Mogensen, Xiang-Yu Huang: Use of GPS observations in an optimum interpolation based data assimilation system

No. 00-15
Mads Hvid Nielsen: Dynamisk beskrivelse og hydrografisk klassifikation af den jyske kyststrøm

No. 00-16
Kristian S. Mogensen, Jess U. Jørgensen, Bjarne Amstrup, Xiaohua Yang and Xiang-Yu Huang: Towards an operational implementation of HIRLAM 3D-VAR at DMI

No. 00-17
Sattler, Kai; Huang, Xiang-Yu: Structure function characteristics for 2 meter temperature and relative humidity in different horizontal resolutions

No. 00-18
Niels Larsen, Ib Steen Mikkelsen, Bjørn M. Knudsen m.fl.: In-situ analysis of aerosols and gases in the polar stratosphere. A contribution to THESEO. Environment and climate research programme. Contract no. ENV4-CT97-0523. Final report

No. 00-19
Amstrup, Bjarne: EUCOS observing system experiments with the DMI HIRLAM optimum interpolation analysis and forecasting system

No. 01-01
V.O. Papitashvili, L.I. Gromova, V.A. Popov and O. Rasmussen: Northern polar cap magnetic activity index PCN: Effective area, universal time, seasonal, and solar cycle variations

No. 01-02
M.E. Gorbunov: Radioholographic methods for processing radio occultation data in multipath regions

No. 01-03
Niels Woetmann Nielsen; Claus Petersen: Calculation of wind gusts in DMI-HIRLAM

No. 01-04
Vladimir Penenko; Alexander Baklanov: Methods of sensitivity theory and inverse modeling for estimation of source parameter and risk/vulnerability areas

No. 01-05
Sergej Zilitinkevich; Alexander Baklanov; Jutta Rost; Ann-Sofi Smedman, Vasiliy Lykosov and Pierluigi Calanca: Diagnostic and prognostic equations for the depth of the stably stratified Ekman boundary layer

No. 01-06
Bjarne Amstrup: Impact of ATOVS AMSU-A radiance data in the DMI-HIRLAM 3D-Var analysis and forecasting system

No. 01-07
Sergej Zilitinkevich; Alexander Baklanov: Calculation of the height of stable boundary layers in operational models

No. 01-08
Vibeke Huess: Sea level variations in the North Sea – from tide gauges, altimetry and modelling

No. 01-09
Alexander Baklanov and Alexander Mahura: Atmospheric transport pathways, vulnerability and possible accidental consequences from nuclear risk sites: methodology for probabilistic atmospheric studies

No. 02-01
Bent Hansen Sass and Claus Petersen: Short range atmospheric forecasts using a nudging procedure to combine analyses of cloud and precipitation with a numerical forecast model

No. 02-02
Erik Buch: Present oceanographic conditions in Greenland waters

No. 02-03
Bjørn M. Knudsen, Signe B. Andersen and Allan Gross: Contribution of the Danish Meteorological Institute to the final report of SAMMOA. CEC contract EVK2-1999-00315: Spring-to.-autumn measurements and modelling of ozone and active species

No. 02-04
Nicolai Kliem: Numerical ocean and sea ice modelling: the area around Cape Farewell (Ph.D. thesis)

No. 02-05
Niels Woetmann Nielsen: The structure and dynamics of the atmospheric boundary layer

No. 02-06
Arne Skov Jensen, Hans-Henrik Benzon and Martin S. Lohmann: A new high resolution method for processing radio occultation data

No. 02-07
Per Høeg and Gottfried Kirchengast: ACE+: Atmosphere and Climate Explorer

No. 02-08
Rashpal Gill: SAR surface cover classification using distribution matching

No. 02-09
Kai Sattler, Jun She, Bent Hansen Sass, Leif Laursen, Lars Landberg, Morten Nielsen og Henning S. Christensen: Enhanced description of the wind climate in Denmark for determination of wind resources: final report for 1363/00-0020: Supported by the Danish Energy Authority

No. 02-10
Michael E. Gorbunov and Kent B. Lauritsen: Canonical transform methods for radio occultation data

No. 02-11
Kent B. Lauritsen and Martin S. Lohmann: Unfolding of radio occultation multipath behavior using phase models

No. 02-12
Rashpal Gill: SAR image classification using fuzzy screening method

No. 02-13
Kai Sattler: Precipitation hindcasts of historical flood events

No. 02-14
Tina Christensen: Energetic electron precipitation studied by atmospheric x-rays